



UNIVERSITÀ DEGLI STUDI DI MILANO - BICOCCA  
Scuola di Scienze  
Dipartimento di Scienza dei Materiali  
Master Degree Course in Materials Science

# **Study of a Method for Battery Cathode Characterization in “Pouch Cell” Format Through Electrochemical Impedance Spectroscopy**

**Advisor:** Prof. Riccardo Ruffo  
**Co-advisor:** Dr. Libero Damen

**Master Thesis Report of:**  
Federico Scarpioni  
Student Number 782347

**Academic year 2018/2019**



# Abstract

Nowadays batteries are a huge business for wide applications: with the diffusion of *electronics devices* are required portable energy storages with high energy density, in the field of *renewable energy* there is the need to store the energy produced to be spent when most needed, the demand for *off grid* and backup power supply units is increasing and, maybe the foremost challenging, the seek for a net-zero carbon footprint *transportation*. So, there is for battery science a double target: *sustainability* and *technology support*.

A battery is a device that store electrical energy in form of chemicals and can reconvert them in direct electrical current via chemical reactions. Essential components are positive electrode, negative electrode, electrolyte, separator and housing (or container). Electrodes are solid-liquid interfaces involved in redox reactions in which the oxidation state of an element changes when electrons are given or taken, they are referred as cathode and anode, respectively. Reactions reagents (ions) are supplied by the electrolyte solution which also allows the ionic current needed to sustain the external electron flux. These components can be hold inside a variety of container geometries, specifically suited for their applications.

A very interesting battery technology for rechargeable systems, is the one that exploits the chemistry of *intercalation*. Lithium ion is the smallest metal ion that brings a single positive charge, is widely available and non-toxic. Li-ion batteries have a transition metal oxide like  $\text{Li}_{0.5}\text{CoO}_2$  and  $\text{LiC}_6$  as positive and negative electrode, respectively. During charge  $\text{Li}^+$  ion is extracted from  $\text{Li}_{0.5}\text{CoO}_2$ , goes into the solution and  $\text{Co}^{3+}$  oxidizes to  $\text{Co}^{4+}$  losing one electron. On the other side of the battery,  $\text{Li}^+$  intercalates between planes of graphite that acquires one electron to balance the charge. Since  $\text{Li}^+$  intercalate and deintercalate in empty position of three-dimensional structures, the reversibility is very high.

The main characteristics of a battery are the *specific energy*, i.e. the power generated in the unit time of an hour per Kg of material, and the *durability* in respect to operating conditions, such as high and low temperature, overcharge and deep discharge, high current, and the loss of lithium by side reaction.

Durability is quantified as number of complete cycles before the charge in the battery drops below 80% of the initial one and is called *capacity retention*. With the term "cycle" is intended a process in which a specific current is maintained between the battery poles and the battery voltage is left free to change between an upper (charge state) and a lower (discharge state) limit; this measurement is thus made in *galvanostatic* conditions. The total charge exchanged between electrodes during the anodic and cathodic processes is considered as the battery *capacity*. At each cycle a small fraction of capacity is lost due to side reactions.

Inside the battery several *mechanisms* take place at different time scales. From fastest to slowest they are: the double layer charging, the ion diffusion in the electrolyte, the adsorption of species onto the electrode surface, the charge transfer between active materials and the environment (current collector and/or electrolyte), the diffusion in the solid state phases and the change of crystalline structure. The time domain of these processes spans from tens of microseconds to hours.

*Electrochemical Impedance Spectroscopy* (EIS) is a non-destructive and fast techniques suitable to investigate all the processes in one experiment. The approach is to stimulate the cell with a small amplitude (< 50 mV) sinusoidal voltage in a wide frequencies range (usually from MHz to mHz). The current induced by the stimulus is collected by the instrument and the impedance is calculated with a computer elaboration software. The results are commonly showed in form of a *Nyquist plot* wherein  $-Z_{Im}$  is reported as a function of  $Z_{real}$ . In the Nyquist plot, semicircles are associated to specific processes and are easily visible and qualitatively evaluable. In this frame, a battery can be assimilated to an electrical circuit, made with basic elements such as resistors, capacitors and inductances connected in series and parallel.

Aim of this work was to build a battery in *pouch cell* format with a third electrode between cathode and anode as a "probe" of potential drop. In this configuration is possible to measure the impedance response of the single interfaces, isolating the processes happening in one electrode of the battery. The function that describes the impedance response of the equivalent circuit of pours electrodes is known from the literature, and the values of the elements of the circuit were obtained from experimental

---

data using a complex nonlinear regression algorithm.

Thanks to the peculiar configuration, the impedances of the cathode and the anode were separately collected and the *Kirchhoff's first law* was verified by summing the impedance of both electrodes, point per point, and overlapping the result to the full cell spectrum, obtained in two electrode configuration.

The focus of the work was the NMC622 cathode, because of the higher interest and margin of discover in respect to the widely studied graphitic anode. The behavior of NMC was studied in respect to *cycle life*, external *pressure* and *temperature*.



# Acknowledgements

I cannot begin without expressing my thanks to my supervisor Libero Damen for the positive cathodic influence on my scientific and personal mindset.

I would like to thank Professor Riccardo Ruffo and Doctor Paula Cojocaru for giving me the opportunity to pursuing my thesis project during an internship at Solvay Specialty Polymers laboratories (Bollate, MI).

I'm deeply in dept with Fabio and Stefano for their spontaneous and indispensable help during my work.

I'm also grateful to Professor Fabio La Mantia for the time dedicated to help me elaborating data and the words of encouragement.

For the patient for my absence in the past months, I should tanks friends and teammates Ian and Sem and the crew of *DefconAces*.

I'm grateful to by *bro* Leonardo for sharing the same joy and sufferings with me during the last years and in particular, together with Giulia and Beatrice, for the quality time during our internship.

I also wish to thanks Costa, Rachele and Alex for the afternoons spent together in front of our laptops, a fireplace and a lot of food. This made me a lot easier to bear MATLAB errors. I need to extent my grateful to all my close friends Simone, Federico, Filippo, Sabrina, Dario, Alessia, Greta, Gabriele, Monica, Alberto and Riccardo for the delightful evenings spent together, all the adventures and the interest on my work progress.

I also want ot express my gratitude to Andrea and Alessandro for taking real care of my stuck on obtaining a working three electrodes battery.

Many thanks to my University colleagues of *El Pueblo* for the incredible support during all the course, inside and outside University walls. Especially outside, in front of a bunch of 1 euro beers. In particular deep thanks to my buddies Matteo and Francesco for they friendship.

Special thanks to Valeria for the mutual help to overcome all the little and big obstacles of the life of young men.

Last but not least I'm extremely grateful to my family, for all the encouraging, the comprehension and tolerance of me screaming in front of the coffee machine before an exam.

# Contents

References . . . . .	1
citerequest	
<b>1 Introduction</b>	<b>11</b>
1.1 Batteries, a big picture . . . . .	11
1.2 Aim of this work . . . . .	12
<b>2 Background</b>	<b>13</b>
2.1 Fundamentals of batteries . . . . .	13
2.2 Batteries characteristics . . . . .	13
2.2.1 Capacity and C-rate . . . . .	14
2.2.2 Energy . . . . .	14
2.2.3 Power . . . . .	15
2.3 Lithium-ion batteries . . . . .	15
2.3.1 Cathode . . . . .	17
2.3.2 Anode . . . . .	17
2.3.3 Electrolyte . . . . .	17
2.3.4 Cell casing . . . . .	18
2.4 Cyclic chronopotentiometry . . . . .	19
2.5 Electrochemical Impedance Spectroscopy . . . . .	20
2.5.1 Fundamentals of the technique . . . . .	20
2.5.2 Basic impedance elements . . . . .	21
2.5.3 Criteria for a valid measure . . . . .	22
<b>3 Metodology</b>	<b>25</b>
3.1 Batteries construction . . . . .	25
3.1.1 Reference electrode preparation . . . . .	26
3.1.2 Assembling procedure of a pouch cell . . . . .	27
3.1.3 Swagelok assembling procedure . . . . .	28
3.1.4 Pressure in cells . . . . .	28
3.2 Cells testing . . . . .	29
3.2.1 Measure the impedance of half cell . . . . .	29
3.2.2 Impedance spectroscopy settings . . . . .	30
3.2.3 Verify a proper cell assembly . . . . .	31
3.2.4 Galvanostatic settings . . . . .	32
3.3 Impedance data analysis . . . . .	32
3.3.1 Preliminarily graphical analysis . . . . .	32
3.3.2 Complex Non-Linear Regression in MATLAB . . . . .	33
3.3.3 The theoretical function . . . . .	33

3.3.4	Validation of impedance spectra . . . . .	36
3.3.5	Quality of regression . . . . .	37
<b>4</b>	<b>Results and comments</b>	<b>41</b>
4.1	Cycling performances of cells . . . . .	41
4.2	Shapes of impedance spectra after cell assembling . . . . .	42
4.3	Shapes of impedance spectra after a current flow . . . . .	45
4.4	Repeatability of EIS measure . . . . .	45
4.5	Effect of the pressure on impedance spectra . . . . .	47
4.6	Stationarity of batteries . . . . .	47
4.7	Effect of the temperature on impedance spectra . . . . .	49
4.7.1	Qualitative analysis of spectra . . . . .	49
4.7.2	Analysis of regression results . . . . .	51
4.8	Effect of the state of charge on impedance spectra . . . . .	54
4.8.1	Qualitative analysis of spectra . . . . .	54
4.9	Electrochemical Impedance Spectroscopy in Swagelok cell . . . . .	55
4.10	Visual inspection of post-mortem cells . . . . .	56
4.10.1	Lithium reference electrode . . . . .	56
4.10.2	The presence of the wire inside the stack . . . . .	57
4.10.3	Mechanical issues from anode formulation . . . . .	58
<b>5</b>	<b>Conclusions</b>	<b>61</b>
<b>Appendices</b>		
<b>Appendix A</b>	<b>MATLAB script for EIS data validation</b>	<b>65</b>
<b>Appendix B</b>	<b>MATLAB script for EIS data regression</b>	<b>71</b>
<b>Appendix C</b>	<b>Results of complex non-linear regressions</b>	<b>77</b>
References . . . . .		79

# 1 | Introduction

## 1.1 Batteries, a big picture

Portable energy sources opened the doors to the electrification of the 21<sup>th</sup> century society. The rapid advancement in science and technology became the engine for industrial and economic growth, bringing to people a more comfortable and convenient way of life. Among all the other portable energy storage technologies (electrochemical capacitor and fuel cell), battery is the most developed technology in the first decades of this century [1] [2]. Batteries are used in a lot of different fields, *portable consumer electronics* [3], *transportation*, *stationary off-grid storage* [5] and *biomedical devices* [4]. The big development, is driven by cost reduction due to scale economy and an extensive research on materials, cell design and processes.

The 88% of battery production came from China, South Korea and Japan [6]. The production chain is composed by material and cell manufacturing, battery pack manufacturing and integration and recycling. To compete with Asia, the rest of the market cannot focus on the same cost-driven starting part of the chain (materials and cell manufacturing) because of the already strong established global market. New opportunities are given for a value-driven strategy in which the focus is on the innovation of cell chemistry, cell format, battery integration, manufacturing technology, processing and recycling strategy.

Lithium-ion batteries are a technology with higher *energy density*. They are widely used in portable electronic devices and in new generation electric vehicles. In the last years governments turn their attention on the development of a framework for lithium-ion batteries development. Europe is making a big effort in this front with the aim of cancel the *carbon footprint* of transportation until 2050 [7].

Cell generation	Cell chemistry	Year
Generation 5	• Li/O <sub>2</sub> (Lithium air)	>2025
Genration 4	• All-solid-state with lithium anode • Conversion materials (primarily lithium-sulphur)	>2025
Generation 3b	• Cathode: HE-NMC, HVS(high-voltage spinel) • Anode: silicon/carbon	~2025
Generation 3a	• Cathode: NMC622 to NMC811 • Anode: carbon (graphite)+silicon comopnent (5-10%)	~2020
Generation 2b	• Cathode: NMC523 to NMC622 • Anode: carbon	Current
Generation 2a	• Cathode: NMC111 • Anode: carbon	Current
Generation 1	• Cathode: LFP,NCA • Anode: carbon	Current

Table 1.1: Europe road-map for battery chemistries [8]; NMCxyz is lithium nickel manganese cobalt oxide  $\text{Li}(\text{Ni}_y\text{Mn}_z\text{Co}_{1-y-z})\text{O}_2$  where  $x+y+z=1$ ; LFP is lithium iron posphate; NCA is Lithium nickel cobalt aluminium oxides  $\text{Li}(\text{Ni}_y\text{Co}_z\text{Al}_{1-y-z})\text{O}_2$ ; [9] .

The Europe road-map for lithium-ion battery materials development is shown in table 1.1. Generation 1 and 2 are the core business at the moment, in large scale production in Asia region. Is not effective to spent effort on mass production on this chemistries. New materials and value beyond cost are the focus of west market.

## 1.2 Aim of this work

Aim of this work was to develop a characterization method for lithium-ion batteries in *pouch cell* format. The novelty of the approach is to introduce inside the device a third electrode to act as a *reference* in electrochemical measure. The use of reference electrodes is an established framework in electrochemical methods but in batteries there is a device engineering challenge that is not yet completely overcame.

The third electrode was introduced to achieve the capability to measure single electrode potentials (anode and cathode) during charge and discharge cycles of te battery and to isolate electrodes contribution to Electrochemical Impedance Spectroscopy measure.

## 2 | Background

### 2.1 Fundamentals of batteries

The battery is a device that store electrical energy in form of chemicals and can reconvert them in direct electrical current via chemical reactions [10]. In its essential, a battery is composed by two electrodes in contact with an electrolyte. Electrodes are solid-liquid *interfaces* involved in redox reactions. A cell is divided in two *half-cells* or *electrodes*. During spontaneous operation (negative free energy), the electrons generated by the oxidation at one interface are transferred to the other for the reduction reaction through an external circuit. Inside the electrolyte, ions (positive and negative) move to maintain the overall charge balance. The electrode where oxidation takes place is called *anode* and where the reduction takes place is called *cathode*. The chemical reactions proceed until one electrode runs out of chemical reagent, at this stage the battery is discharged. If the redox reactions are *reversible*, the cell can be restored to initial condition, or *recharged*. This type of devices are called *secondary batteries* or *rechargeable* in opposition to *primary batteries* or *non rechargeable*. Recharging a battery is a non-spontaneous process (positive free energy) and it is led by an external power source. During this process oxidation and reaction happen at the opposite half-cell than before and the external current change sign, however the names of the electrodes remain unchanged for simplicity [11].

### 2.2 Batteries characteristics

Batteries are characterized by three main properties: *capacity*, *energy*, *power*. This characteristics are usually express for unit

of active material's weight (kg or g) or volume. In such a way different material can be compared to address the most suited for a specific application [10].

### 2.2.1 Capacity and C-rate

Capacity is the amount of charges stored in the bulk of active material. It is calculated with:

$$Q = x(nF) \quad (2.1)$$

where  $x$  is the total number of moles of reaction associated with the complete discharge of the cell,  $n$  is the stoichiometric number of electron exchanged and  $F$  the Faraday's constant ( $9.65 \cdot 10^4 \text{ A s mol}^{-1}$ ). Capacity is a property of the electrode. When two electrodes are coupled together to build a battery the amount of materials is calculated to have a *balanced* capacity. Most of the time the ratio between anode and cathode is not unitary but can be between 1.03 or 1.2 for a longer cell lifetime and safety reasons [12]. Capacity is measured in Ah, Ah/kg or Ah/dm<sup>3</sup>.

*C-rate* is a closely related parameters widely used in battery testing. It is defined as the rate (1/time) at which the cell completely discharge or charge at a constant current. In other words is the ratio of the current load and the capacity:

$$C\text{-rate} = \frac{I}{Q} = \frac{[A]}{[Ah]} \quad (2.2)$$

The C-rate is measured in h<sup>-1</sup> and it is expressed with the formula  $mC$  where  $m$  is the number of hours required to charge or discharge the cell. For example 2C means that the battery is charged or discharged in half an hour and  $C/2$  means that the process requires 2 hours.

### 2.2.2 Energy

Energy is the most used parameter to compare cells. Theoretical energy is

$$\mathcal{E}_T = x(nFE_{cell}) \quad (2.3)$$

where  $E_{cell}$  is the *electromotive force*, that is the potential of the cell under load. This value depends on the electrodes materials thermodynamics and condition of operation (kinetics). The real energy during discharge depends on the real capacity extracted

from the cathode that can vary a lot from the theoretical one:

$$\mathcal{E}_P = \int_0^{xnF} Edq \quad (2.4)$$

where E is the actual potential of the system that change with *state of charge* (or SOC).

Energy is measured in Wh, Wh/kg or Wh/dm<sup>3</sup>.

### 2.2.3 Power

Power is defined as:

$$P = I \cdot E \quad (2.5)$$

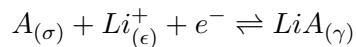
Current I depends on the external load of the cell. When the current is to high the system is not capable of sustain the flux of electrons and the cell potential E drops, reducing the power produced. In fact current flux through electrodes interphase produce a polarization effects called *overpotential* [11].

Power is measured in W, W/kg or W/dm<sup>3</sup>.

## 2.3 Lithium-ion batteries

*Lithium-ion batteries* are the category of batteries with the highest energy density. To compare storage systems a *Ragone chart* came in handle, see figure 2.1. As the figure show, lithium-ion batteries can be tuned for every type of application, from low to high power, sacrificing some specific energy. To choose the correct material for an application is also important to evaluate its operating voltage and the capacity which both depend on the chemistry.

In a lithium-ion battery, an active material A undergoes a reversible electrochemical reaction with lithium ion from the electrolyte:



Note that the phase of the material (in subscript) can change for the active material, electrolyte solution is represented as phase  $\epsilon$ . Now the question is to find suited active material, lithium sources and electrolyte to build the battery. Each component will be briefly covered in the follow.

When an electrode is put in contact with an electrolyte solution (polar or polarizable)<sup>1</sup>, the molecules of the solvent

1: This is a general behavior of all kind of interfaces.

rearrange in the interface in an ordered plane of dipoles producing a charged surface. The metal electrode have free electrons that react moving further or away the interface, forming a plane of charge with opposite sign than the one in the electrolyte [41]. The final system is like a plane capacitor and a potential difference is established proportional to the number of charges separated, this is the *electrode potential*. This potential depends on the nature of the materials and their thermodynamics.

When a battery is operating, electrons and ions cross the interfaces generating a polarization voltage opposite to the equilibrium electrode potential. This is called *overpotential*. Furthermore the viscosity of the solution influences the mobility of ion in the electrolyte and another contribute to the voltage is added, usually called *electrolyte Ohmic drop*.

When cathode potential is measured in respect to the anode, the value of the cathodic overpotential is not appreciable because of the presence of an unknown anode overpotential. When the cathode potential is measure in respect to another electrode with constant potential during time and independent on the current flowing in the battery, the absolute value (or respect pseudo-reference electrodes) is revealed.

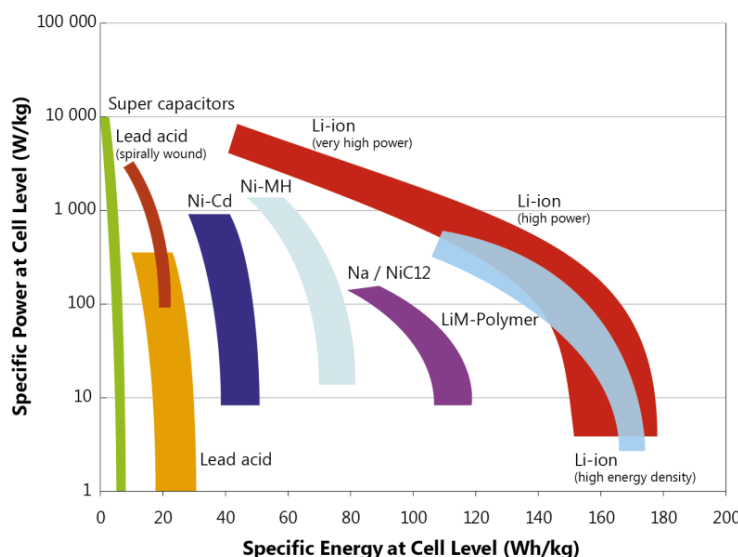


Figure 2.1: Ragone chart to compare different storage technology: supercapacitors and different battery chemistries; image from Scott Lemon and Allan Miller. “Electric Vehicles in New Zealand: Technologically Challenged?” In: June 2013.

### 2.3.1 Cathode

Battery cathodes are usually transition metal oxide. Lithium-ion is exchanged when the transition metal is oxidized or reduced to maintain charge balance in the material. The most used material at the moment is the layered structured  $\text{LiMnO}_2$  [14], in particular at the chemistries where Mn is partially substituted with Ni and Co:  $\text{Li}(\text{Ni}_y\text{Mn}_z\text{Co}_{1-y-z})\text{O}_2$  [15]. These materials are called "NMCxyz". Best performance are shown from materials with  $y=z$  [16], at the moment the most interesting material industry materials is  $\text{Li}(\text{Ni}_{0.6}\text{Mn}_{0.2}\text{Co}_{0.2})\text{O}_2$  or NMC622, but NMC811 is the upcoming chemistry for the next months. NMC622 have a specific capacity of 276.5mAh/g and an equilibrium potential window of  $\sim 3\text{-}4.7\text{V}$  vs  $\text{Li}/\text{Li}^+$  [17].

### 2.3.2 Anode

The anode material with the highest capacity is metallic lithium with 3860 mAh/g [18], lowest density ( $0.534 \text{ g cm}^{-3}$ ) and lowest potential of  $-3.040\text{V}$  vs *standard hydrogen electrode* (SHE). The use of lithium is challenging because it is thermodynamically unstable in electrolytes during cyclation and when the lithium ions reduce at the surface of metallic lithium, they tend to form dendrites and cluster that reduce capacity and damage the cell components (ex. perforating the separator and cause short-circuits). The latter phenomenon is called *lithium plating* and it is always to avoid. The most used material for anode is carbon [14], lithium ions can *intercalate* between graphite plane in a reversible process. The capacity of graphite is 372 mAh/g and it has 3 potential plateau at 0.2V, 0.12V and 0.08V vs  $\text{Li}/\text{Li}^+$ , therefore it is safe to use a lower potential limit of 60mV vs  $\text{Li}/\text{Li}^+$  to avoid plating.

Next generation of materials are alloying materials like Si and Sn. [19].

### 2.3.3 Electrolyte

The Electrolyte is a solvent containing partially dissociated salt to provide ions for support the external current avoiding electronic conductivity inside the cell. Most used and commercially available are cyclic carbonates in presence of additives and  $\text{LiPF}_6$  as salt. *Ethylene carbonate* (EC) is a cyclic solvent with high *dielectric constant* (low electrical conductivity) and low viscosity, but it is solid at room temperature so it is mixed with linear

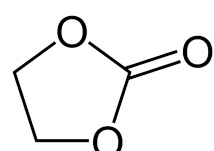


Figure 2.2: Ethylene carbonate molecule.

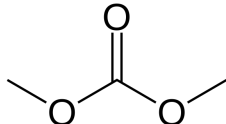


Figure 2.3: Dimethyl carbonate molecule.

solvents like *dimethyl carbonate* (DMC). A 1:1 mix is widely used to produce 1M LiPF<sub>6</sub> solution. Carbonates have a high temperature range and electrochemical window but the ionic conductivity is lower than aqueous solutions, below 10mS/cm.

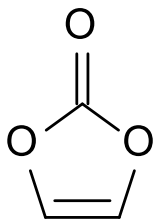


Figure 2.4: Vinylene carbonate molecule.

The electrolyte is soaked into a porous separator that guarantees electrodes separation (to avoid short circuits) and maintains a wet interface. As separators can be used semi-crystalline polyolefine materials, non-woven fiber mats or inorganic composites [20]. There are a lot of aspects to be considered like thickness, porosity, pore size, permeability, strength, wetability, thermal shutdown and cost. Commercial batteries use polyolefine separator for the very low thickness, down to 10μm, low cost and overall good performances. The presence of a separator is essential but it reduces the ionic conductivity of the electrolyte by as much as one order of magnitude [21].

Electrodes are not thermodynamically stable in organic electrolyte, but when they are in contact the first time, a layer of partially decomposed and polymerized carbonates with lithium in various form, isolate material for further degradation [22]. This passivation layer is called *solid electrolyte interface* (SEI) and its formation is stabilized by the presence of *vynilene carbonate* (VC) in solution, see figure 2.4 [23]. A stable SEI is grown in the first cycle of the battery at low C-rate, some of the capacity is lost in this layer, but during cell operation it does not expand further [24].

### 2.3.4 Cell casing

Battery components can be held inside different casings with their own geometries. Manufacture cell types are the prismatic, cylindrical, coin and pouch cells [14], see figure 2.5. First three have an hard aluminum case, instead the pouch cell have aluminized plastic bag that gives, lightness, flexibility and shape versatility compared to the others form factor. In research laboratories, custom cells are home built to meet the individual purpose. Most known are Swakelok or "T-type" cells, which is a generic name to indicate cells with 2 or 3 way pressurized air junction as case, and *ECC* cells sold by EL-Cell [25].

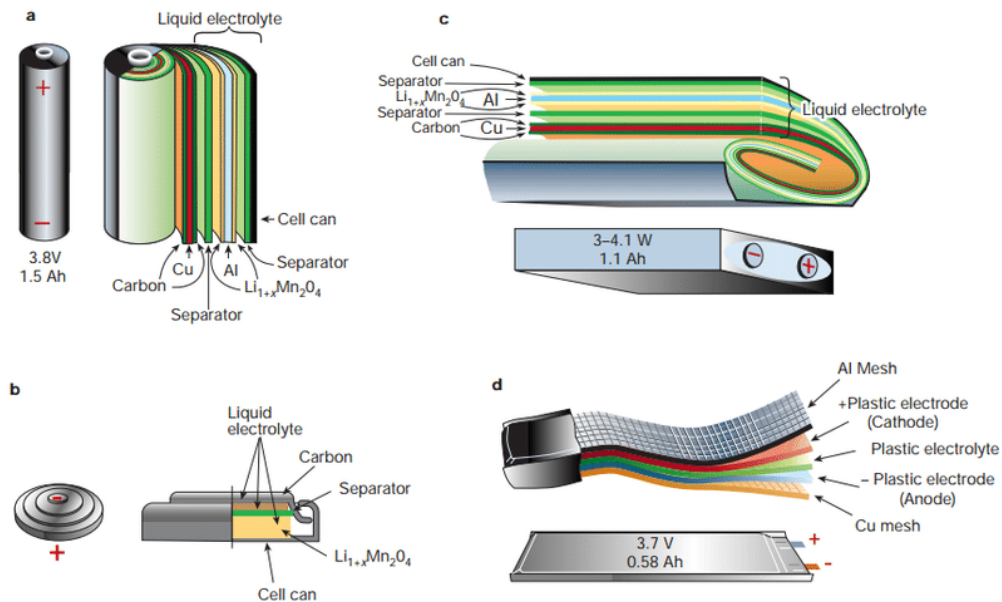


Figure 2.5: Cases for commercial batteries; a) cylindrical; b) prismatic; c) coin; d) pouch, image from Yemeserach Mekonnen, Aditya Sundararajan, and Arif Sarwat. “A review of cathode and anode materials for lithium-ion batteries”. In: Mar. 2016, pp. 1–6. DOI: 10.1109/SECON.2016.7506639

## 2.4 Cyclic chronopotentiometry

*Chronopotentiometry* belongs to controlled-current techniques also named *chronoamperometric* or *galvanostatic* techniques. A constant current is supplied by a *galvanostat* and the potential of the cell is recorded with an acquisition device. In battery science, current is provided or drained to charge or discharge the cell at a constant rate (it is usually used the C-rate term) and the potential evolution of electrode is evaluated. Usually cut-offs for maximum and minimum voltage are used to prevent damage to cell materials. A qualitative example is depicted in figure 2.6. During each step the number of electrons is counted to obtain the charge and discharge capacities which are always less than the theoretical one. The ratio between charge and discharge capacities is called *Coulombic efficiency* and is a performance parameter of the device.

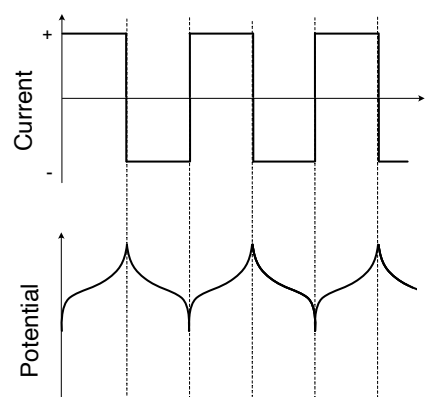


Figure 2.6: Current and full cell potential profile during a cyclic chronopotentiometry, qualitative representation.

## 2.5 Electrochemical Impedance Spectroscopy

### 2.5.1 Fundamentals of the technique

In electromagnetism *electrical impedance* is the measure of the opposition that a circuit present to an alternate current  $i$  when an alternate voltage  $v$  is applied. Similar to the Ohm's law in mathematical term impedance is defined:

$$Z(\omega) = \frac{v(\omega)}{i(\omega)} \quad (2.6)$$

*Electrochemical Impedance Spectroscopy* (EIS) is a non destructive, easy and fast technique that is able to discriminate kinetic processes happening at different time scales and to obtain the time constant of each one. During an experiment, a controlled *sinusoidal* voltage or current is supplied to the system and the correlated quantity is measured to compute impedance [26]. When the input is voltage the technique is referred as *Potentiostatic Electrochemical Impedance Spectroscopy* (PEIS) and *Galvanostatic Electrochemical Impedance Spectroscopy* (GEIS) when the input is current. In the *linear* region (see next section) the results is the same for both operation mode, the choose depends on which quantity needs to be controlled in a specific system. The input is controlled and response can be whatever value, in some cases can be unwanted, for example, to have high current pulses.

To perform an EIS experiment, a potentiostat or galvanostat paired with a sine wave generator is needed to generate the stimulus and a response analyzer like an *oscilloscope* or a more sophisticated *Frequency Response Analyser* units (FRA) [27]. Modern electrochemical instrument are all-in-one devices.

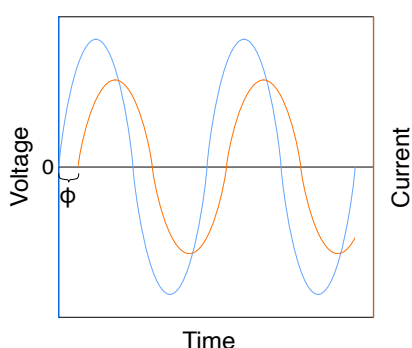


Figure 2.7: Qualitative representation of a sinusoidal voltage input (blue line) and phase shifted current output (orange line) of a system.

Sinusoidal function have the form

$$v(t) = V_0 \cdot \sin(\omega t) \quad (2.7)$$

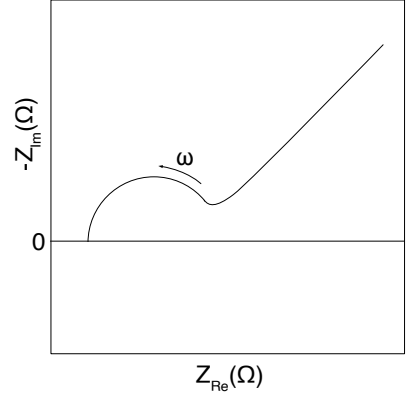
$$i(t) = I_0 \cdot \sin(\omega t + \phi) \quad (2.8)$$

where  $V_0$  and  $I_0$  are maximum amplitude and  $t$  is time. The system opposes to the input and the output quantity is reduced in amplitude and/or shifted in phase, see figure 2.7. The phase  $\phi$  is added to the argument of sine of the output. The experimental apparatus manage current and voltage as a function of *time*, but

impedance in equation 2.6 is a function of angular *frequency* (*time* =  $2\pi/\omega$ ). To obtain impedance, voltage and current must be *transformed* from time to frequency domain using *Fourier transform* [26], given a function of time  $f(t)$  its transform is:

$$F(\omega) = \frac{2}{T} \int_0^T f(t) e^{-j\omega t} dt \quad (2.9)$$

where  $T$  is the period of the periodic function and  $j$  the *imaginary unit*. Impedance is therefore a *complex quantity* and can be written as  $Z = Z_{Re} + jZ_{Im}$ . The most common visual representation of impedance is through a *Nyquist plot*, see figure 2.8, but exist also another representation called *Bode diagram*. The negative imaginary part of the impedance is reported as a function of the real part.



## 2.5.2 Basic impedance elements

In the follow will be illustrated the impedance of basic impedance elements. This elements are important because they can be arranged to build a circuit that have the same response of an electrochemical system. The representation of these elements in a Nyquist plot is reported in figure 2.9. Derivation of the following relation can be found in electromagnetism and electronics textbooks.

### Resistor

Resistor's impedance is independent on the frequency and it is equal to the resistance value, in the Nyquist plot it is a point on the x-axis:

$$Z(\omega) = R. \quad (2.10)$$

### Capacitor

Ideal impedance of a capacitor have non real negative part that converges to zero for high frequencies:

$$Z(\omega) = -\frac{1}{j\omega C}. \quad (2.11)$$

### Inductor

Ideal inductor of a inductor have non real positive part that converge to zero at low frequency:

$$Z(\omega) = j\omega L. \quad (2.12)$$

Figure 2.8: Example of an impedance spectrum represented in a Nyquist plot.

### RC circuit

The impedance of a resistor and capacitor in parallel is a semi-circle. The diameter is the resistance value of the resistor and the capacitance is calculate from the maximum frequency  $\omega_{max}$ .

$$\omega_{max} = \tau = R \cdot C \quad (2.13)$$

where  $\tau$  is the time constant of the circuit. The complex impedance of this element is:

$$Z(\omega) = \frac{R}{1 + j\omega\tau}. \quad (2.14)$$

In real electrochemical systems, typically the semicircle is depressed, with the center with positive imaginary part. The capacity is replaced with a *constant phase element* (CPE) with symbol Q [28]. The impedance of RQ circuit is :

$$Z_Q = \frac{R_{RQ}}{1 + (j\omega\tau_{RQ})^a}, a = [0, 1]. \quad (2.15)$$

When  $a$  is equal 1, this element represent a pure capacitor, when  $a$  is 0 it represent a pure resistor and when  $a$  is 0.5 it is a *Warburg element*.

### Warburg Element

The Warburg element describe a semi-infinite diffusion, its impedance is described with the following equation [29]:

$$Z_W(\omega) = R_W \cdot \frac{\tanh(j\omega\tau_W)^{a_W}}{(j\omega\tau_W)^{a_W}}. \quad (2.16)$$

The physical interpretation is that this circuit represent the diffusion length. In order to pass a length element, a certain amount of work is necessary (modeled by the resistor). In addition to this, some overconcentration can be stored in each length element (modeled by the capacitor) [30].

### 2.5.3 Criteria for a valid measure

A valid Electrochemical Impedance Spectroscopy measure must fulfill three criterion:

- causality;

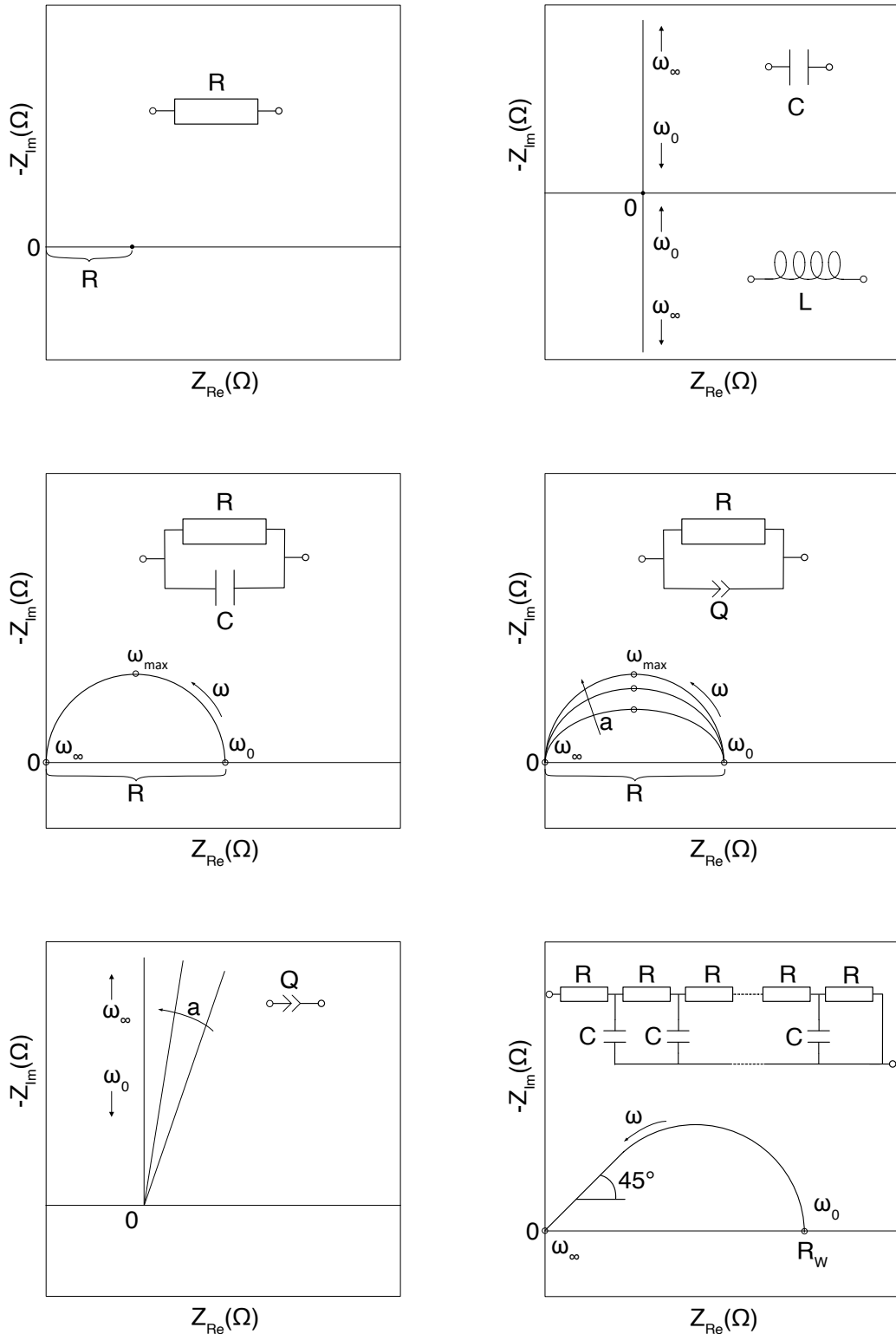


Figure 2.9: Impedance of different electric elements reported in Nyquist plots.

- linearity;
- stability.

*Linearity* means that the current-voltage relation must be linear, i.e. the stimulus amplitude have to be sufficiently small to produce an impedance response independent from the chosen amplitude. A too high stimulus can interfere with the kinetic of the system and the response signal would be biased. *Causality* means that the response of the system is only dependent on the system characteristic and *stability* means that during the measure the system must not evolve.

# 3 | Metodology

In this chapter are described:

- procedures used to build pouch and Swagelok cell types;
- settings used for Electrochemical Impedance Spectroscopy and chronopotentiometry;
- algorithms used for EIS data validation and non-linear regression of theoretical impedance function with MATLAB.

This work was a continuing improvement, during each assemble and test something new was introduced based on previous experience, therefore same measure have different settings. The performances of a cell was evaluated in term of shape and resistance value of impedance spectrum, potential profile of galvanostatic charge and discharge and post mortem visual inspection of electrodes.

## 3.1 Batteries construction

Using the same electrodes batteries with two geometries were assembled. *Monolyerd pouch cell* because of the similarities with a commercial battery, see figure 3.1 and *Swagelok*, see figure 3.2. The letter was used as a comparison to verify that the response of the cell does not depend on the cell geometry. Main differences between the two are the capacity, which is function of the electrode area, 36mAh for the pouch cells and 3.4 mAh for the Swagelok cells, and the thickness of the separator, 20 $\mu$ m for the pouch cells and ca. 1mm for the Swagelok cells. For the pouch type cell the working area is a rectangle of 12cm<sup>2</sup> and for the Swagelok type cell the area is a disk of 1.13cm<sup>2</sup>.

Materials used to build cells are summarized in table 3.1. Electrodes and glass microfiber filters were dried in a Büchi

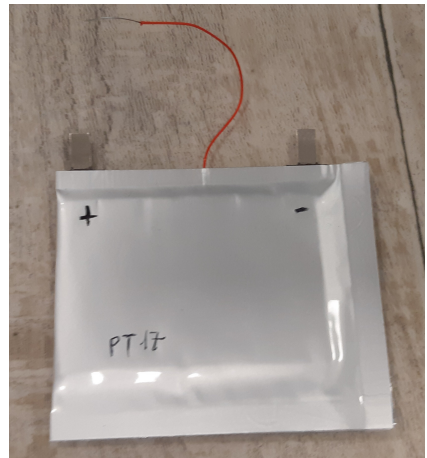


Figure 3.1: Photo of a three electrode pouch cell

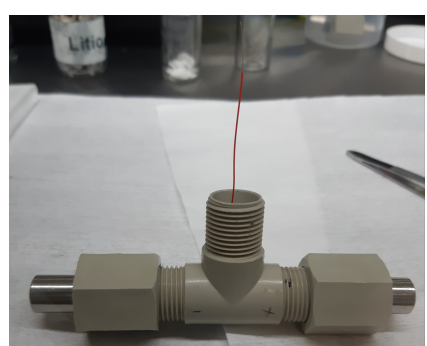


Figure 3.2: Photo of a three electrode Swagelok cell

Battery component	Materials and composition	Productor
Cathode	95% wt LiNi <sub>0.6</sub> Mn <sub>0.2</sub> Co <sub>0.2</sub> O <sub>2</sub> , 3% wt SuperP carbon black (Timcal), 2% wt PVdF. Current collector: aluminum foil 15µm thickness (Solvay EWHA), alluminum tab. Produced in NMP.	Ulsan Technopark
Anode	96.5% wt graphite, 1.5% wt SBR, 1% wt SuperP carbon black (Timcal), 1% wt CMC. Current collector: copper foil 11µm thickness (Solvay EWHA), nickel tab. Produced in MilliQ water (Merk Millipore).	Ulsan Technopark
Separator for pouch	Tonen micropourus polyethylene 20µm thickness, porosity 45%.	Toray
Separator for Swagelok	Watman glass microfober filter 0.66mm (x2).	Sigma-Aldritch
Electrolyte	LiPF <sub>6</sub> 1mol in EC:DMC (1:1 wt) + 2% VC (for pouch). LiPF <sub>6</sub> 1mol in EC:DMC (1:1 v) + 2% VC (for Swagelok).	Solvionic
Reference electrode	99.9% Lithium	Alfa Aeser
Reference electrode	PVdF Kynar insulated copper wire with silver coating. Metal diameters of 0.25mm and 0.5mm external diameter. It support a maximum of 300V, 400mA and 130°C in operation.	RS PRO

Table 3.1: Materials used in cells.

Glass Oven (B-585 Drying) at 130°C overnight and polyethylene separator at 70°C overnight. All components were kept in an argon filled glove-box (from MBrown) with less than 0.5 ppm of water and oxygen.

More than twenty pouch cells were assembled, but the most interesting data, discussed in next chapter, were obtained from four cells.

### 3.1.1 Reference electrode preparation

As reference electrode was used metallic lithium connected outside the cell through an insulated copper wire. Wires 8cm long were prepared and the PVdF<sup>3</sup> insulation was removed from both ends, with the help of a soldering iron at 250°C that melt the polymer. Copper metal was exposed for a lenght of 1-2mm at

3: Polyvinylidene fluoride

one side (lithium end) and 2cm for other other(external end) . The available copper wire was coated with silver by production and this coating was removed dipping the tip of the wire into a 10%vol HNO<sub>3</sub> water solution for few seconds. When silver is all removed the dissolution of copper begins and the solution turn to green around the metal end. The silver presence is to avoid because of the unstable potential and the capability to alloying with lithium altering its potential [31]. Then to the exposed copper was applied a small quantity of metal lithium, sufficient to cover all the copper. Note that lithium sticks better on the PVDF than copper, so it's useful to make lithium slightly overlap the coating. The wire was rolled over a plastic plane to smooth the surface and then surface was scrapped with a spatula to obtain a shiny look as reported by Burrows and Jasinski [32]. The reference electrode obtained is a lithium cylinder with an height of 2mm circa and a base of 0.5mm. The exposed area is :

$$\begin{aligned} \text{Area} &= 2\pi \cdot \text{radius} \cdot \text{height} \\ &= 2\pi \cdot 1\text{mm} \cdot 0.5\text{mm} = 3.14\text{mm}^2. \end{aligned} \quad (3.1)$$

### 3.1.2 Assembling procedure of a pouch cell

Electrodes were die-cutted from a sheet in rectangular shape as shown in figure 3.3. The dimensions of the anode are slightly bigger to help alignment. For each electrode the active material was removed from the 5x5mm area outside the rectangle scrapping it with a spatula and the exposed metallic surface was cleaned with acetone. The tab was then welded in this cleaned area with a ultrasonic welding machine (MTI Corporation, model MSK-115A). Electrodes were then dried and transferred in glovebox. The anode was attached to the separator using a Kapton tape then another piece of separator was attached to protect the cathode from the reference. The cathode was positioned on top and fixed in place with tape. See figures 3.4 for a schematic structure of the battery. Two pieces of PTFE<sup>4</sup> were added on top both electrodes to keep angularity. The piled structure was then put inside a plastic bag and three of four sides were sealed with a vacuum-sealing machine (MTI, MSK-800). The tabs used (from MTI) had a strip of thermoplastic tape already applied, so for the copper wire a piece of thermoplastic tape (from MTI) was position in the sealing zone to ensure a correct adhesion of both sides of the plastic bag without voids. An excess of electrolyte was slowly poured with a micropipette keeping the tip in contact with the separator to ensure best percolation inside pores and three stages of low-pressure treatment was performed to

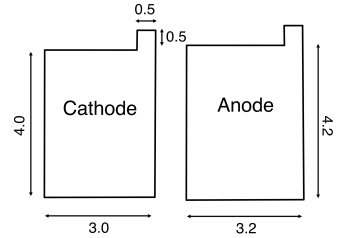


Figure 3.3: Dimensions of electrodes used.

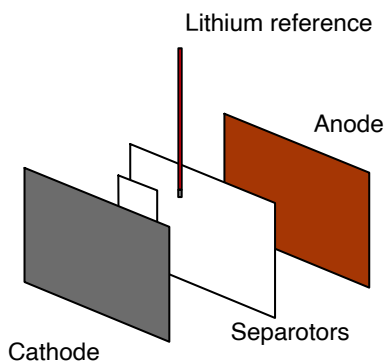


Figure 3.4: Schematic representation of pouch cell stacks; isometric view.

4: Polytetrafluoroethylene

expel argon from pores. The last side of the pouch was then sealed setting a pressure of -90Pa in the sealing chamber. Before testing, cells were kept in rest for 10 hours.

### 3.1.3 Swagelok assembling procedure

To assemble a Swagelock type cell a *T-shaped* three ways junctions for pressured air in polypropylene (PP) were used. All components of the battery were staked and pressed together through a couple of steel cylinders. The reference electrode was positioned between two glass fiber filters (0.66mm each). Cylinders where kept in position using a gasket and a PP nut. The battery stack with cylinders was inside the 2 coaxial extremities. The third perpendicular extremity was used for the reference electrode and the entrance closed with Parafilm to prevent electrolyte evaporation. The cells were kept in rest for 10 hours before testing.

### 3.1.4 Pressure in cells

A good contact of electrodes with separator is needed for the best performing of a battery. In Swagelok cells all the components are pressed together between the two steel cylinders with the pressure applied by the operator. Inside a pouch cell, components are kept under the external pressure of only 90Pa because of the vacuum applied during the cell preparation. A study of the best pressure for optimal cell performance was not a topic of this work, but as reported by Mussa et al. [33] a pressure around 1.3MPa is the beneficial for cycling life compared to atmospheric pressure or a too high pressure and affect cell resistance. Impedance Spectroscopy measures was performed with different set-up to see the effect of the pressure. Pressure was applied using metallic weights and two paperclips like the ones in figure 3.5. It was calculated that a weight of 622g produces a pressure of 2.7KPa and a weight of 793g a pressure of 3.4KPa. The value of the pressure exercised with paperclips was not evaluated, but is considerably higher than the weights. From other laboratory experiments is known that two-electrodes pouch cells with same materials perform very well with paperclips, with an excellent capacity retention cycling at 1C.



Figure 3.5: Office paperclips used to keep cells in pressure.

5: Conductive polymer around a structural fabric inner.

To have a well distributed pressure under paperclips, the cell was put between two pieces of lamination pad<sup>5</sup> (Cardlam 220 by Cardel) and two acrylic plates, see figure 3.6A. Since the

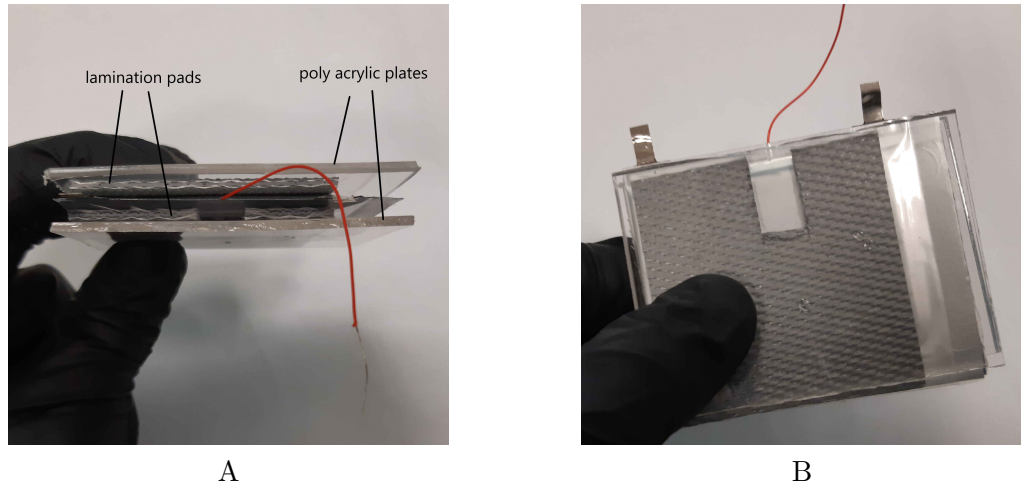


Figure 3.6: Pouch cell pad for pressure; A) top view, B) front view, the cut in the pad for reference is visible.

reference electrode wire is more than 10 times thicker than the separator, few short-circuits were occurred until a cut of the silicon pad was performed, see figure 3.6B.

## 3.2 Cells testing

Impedance spectroscopy and chronopotentiometry were performed using a BioLogic VMP-3 and BioLogic SP-150, with EC-Lab software updated to version 11.30. The majority of measures were performed in a room with an air conditioning set at 24°C which is not entirely sufficient to maintain a stable temperature; in this work it will be referred to this condition as *room temperature*. Some measurements were instead performed at controlled temperature using a ventilated laboratory oven (from Binder), the temperature will be specified in each case in the discussion of results.

### 3.2.1 Measure the impedance of half cell

To describe how impedance were performed, a simplified representation of a battery will be used, see figure 3.7. All the phenomena occurring, are included in two resistors,  $R_1$  for the left side of the cell and  $R_2$  for the right side, which include the resistance of the electrode and half of the electrolyte. Furthermore it is supposed that the voltage drop inside the cell is simply linear. The impedance of the whole system is measured

Parameter	Value
Frequency range	100 KHz-10mHz
Amplitude	15mV
Waiting period	1
Measurement periods	3
Drift correction	ON

Table 3.2: Best parameters found for EIS for pouch cells

6: Note that inverting the order of the wiring WE and CE will not change the response of the system since the input is oscillating.

connecting the working terminal of the potentiostat to electrode  $E_1$  and both counter and reference terminals (short-circuited together) to electrode  $E_2$ <sup>6</sup>. This is called a *two-electrodes measure*. For a specific frequency the instrument will measure a voltage  $V_{WE-CE}$  and a current  $I$  and the resulting impedance is:

$$\frac{V_{WE-CE}}{I} = R_1 + R_2, \quad (3.2)$$

in other words all the contributions are measured.

To obtain the impedance of a half-cell the reference terminal must be placed in a position between the electrodes, for example in the middle to see exactly half of the electrolyte resistance per half-cell. This configuration is called a *three-electrodes measure*. The instrument will measure the voltage  $V_{WE-RE}$  and the current  $I$  giving the impedance:

$$\frac{V_{WE-RE}}{I} = R_1; \quad (3.3)$$

the contribution of the left side is isolated. To obtain the impedance of the electrode  $E_2$ , working and counter cables must be simply reversed.

### 3.2.2 Impedance spectroscopy settings

The best settings found to obtain a good impedance spectrum for battery electrodes is reported in table 3.2. The range is sufficient to start see the diffusive part and the amplitude is enough to have noise-free spectra but sufficiently small to retain linearity. Only for the Swagelok cell it was possible to reach 200KHz without see any inductive loops. After a change of state of charge or temperature, the system gets out of equilibrium. To measure a good impedance spectrum it is convenient to let the cell relax for a certain time. For the change of SOC it was chosen to wait 2 hours and for a temperature increment of 10°C,

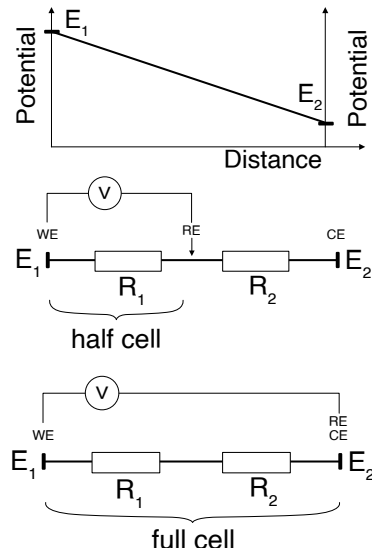


Figure 3.7: Schematic representation of two and three electrodes impedance measure.

1 hour was left. These numbers came after the observation of the drift of the potential in open circuit. A more robust procedure to address the correct rest time is presented by Wang et al. [34].

A measure with the parameters reported requires more than one hour to be completed. These parameters were adopted in the second half of the work, for the first part a shorter range (up to 100mHz) was used and no drift correction or waiting period was exploited.

For the stimulus amplitude were used 5mV at the beginning of the work, then 15mV were used because was verified that linearity persist and using a bigger stimulus increases the signal to noise ratio.

### 3.2.3 Verify a proper cell assembly

After assembling a cell the value of potentials and analysis of the impedance spectra assess a proper manufacture. Graphite must be around 3.2V when measured in respect to the lithium reference, NMC is around 150-180mV respect graphite and so one have to see around 3.35-3.38V between cathode and reference.

In second place the proper position and functionality of the reference can be tested with impedance spectroscopy: the impedance of the full cell must be equal to the sum of the impedances of anode and the cathode, as the *First Kirchhoff's circuit law* asserts.

In figure 3.8 is represented this summation of cathode and anode spectra in comparison to the full cell for a pouch cell. The value  $\Delta$  is the difference of the sum with respect to full cell and it is calculated using the formula:

$$\Delta(\%) = \frac{1}{N-1} \cdot \sum_{i=1}^N \frac{|Z_{Re}^{Full}(\omega_i) - Z_{Re}^{Sum}(\omega_i)| + |Z_{Im}^{Full}(\omega_i) - Z_{Im}^{Sum}(\omega_i)|}{Z_{Re}^{Full}(\omega_i) + Z_{Im}^{Full}(\omega_i)} \cdot 100, \quad (3.4)$$

where  $N$  is the number of points acquired (i.e. frequencies),  $Z_{Full}(\omega_i)$  is the impedance of the full cell and  $Z_{Sum}(\omega_i)$  is the sum of the impedance of cathode and anode.

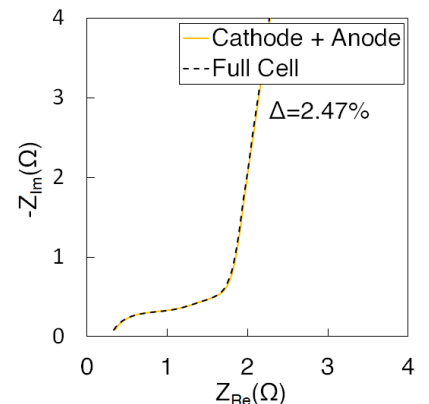


Figure 3.8: Impedance of a pouch cell after assembling.

### 3.2.4 Galvanostatic settings

The SEI formation step was conducted at C/20 at room temperature. For successive steps a current corresponding to C-ratio of C/10, C/4 and C/2 were used to evaluate cell performance in different conditions (current regimes). For the two-electrode configuration the cell was cycled using the GCPL1 protocol of EC-Lab software with potential between 3V and 4.2V with a potentiostatic step in charge and discharge until the current dropped to C/50. A point was acquired every 30 seconds or after a change of potential change of 50mV.

For three-electrode configuration the GCPL2 protocol was used because it permits to set different cut off values for both electrodes. For the cathode lower and upper limits were 3V and 4.3V and for the anode 0V and 1V respectively.

After assembling and first impedance each cell was kept in open circuit measuring the voltage for working, counter and reference. In this step it is possible to evaluate drifts due to equilibration of the system or identify errors in the reference behavior.

## 3.3 Impedance data analysis

### 3.3.1 Preliminary graphical analysis

When non-overlapping semicircular arcs appear in the spectrum, resistance and capacitance values associated to a process can be extracted. The frequency at the peak of the arc is the reciprocal of time constant of the process:

$$\omega = \tau^{-1} = (RC)^{-1}. \quad (3.5)$$

Instruments software like EC-Lab have an integrated capability to perform circular fit on user selected data and automatically calculate high and low intercept of arc and parameters values. This approach is only a preliminary investigation, it can tell nothing about overlapped semicircles. More information can be extracted using a physical model and a regression algorithm.

### 3.3.2 Complex Non-Linear Regression in MATLAB

Regression is a statistical analysis concept in which an algorithm look for the best parameters of a theoretical function  $f(x, \mathbf{P})$  to most closely fit experimental data. When a function of one or more variable is a non-linear combination of parameters, the process is called non-linear regression.

In a *complex* non-linear regression, real and imaginary part of a *complex model function* involving a set  $\mathbf{P}$  of  $n$  unknown parameters, are regressed simultaneously over complex data. A standard method to approximate the solution of overdetermined systems<sup>7</sup> is the *least squares* [36]. Let call  $f_{i,data} = f'_{i,data} + j f''_{i,data}$  the data set, where  $i = 1, 2, \dots, N$  with  $N$  number of frequencies (or points collected), and  $\hat{f}(\omega_i, \mathbf{P}) = \hat{f}'(\omega_i, \mathbf{P}) + j \hat{f}''(\omega_i, \mathbf{P})$  point from the theoretical function. The least squares procedure involve the minimization of the sum of squares function:

$$S(\mathbf{P}) = \sum_{i=1}^N \frac{\left[ f'_{i,data} - \hat{f}'(\omega_i, \mathbf{P}) \right]^2 + \left[ f''_{i,data} - \hat{f}''(\omega_i, \mathbf{P}) \right]^2}{(f'_{i,data})^2 + (f''_{i,data})^2}. \quad (3.6)$$

The function  $S$  is generally called *object function*.

Minimization procedure is a mathematical *optimization problem* and in this work was carried using MATLAB 2018b and the function `fminsearchbnd` that is a modified version of `fminsearch` with the possibility to include upper and lower limit to each parameter [37]. The code was written in-house and it is reported in appendix ???.

An optimization function requires adequate starting parameters. This is a very delicate question because with wrong starting points the process could bring to a local minimum point of the function or non physical meaningful parameters. Since the the theoretical function, topic of the next section, is deduced from an equivalent circuit, values of circuit elements can be predicted from the graphical analysis of the impedance spectrum (3.3.1).

### 3.3.3 The theoretical function

The theoretical function used, which represent cathode impedance, was the one proposed by Landesfeind, Pritzl, and Gasteiger [35]

7: Systems in which the numberer of equations is more than the number of unknown parameters.

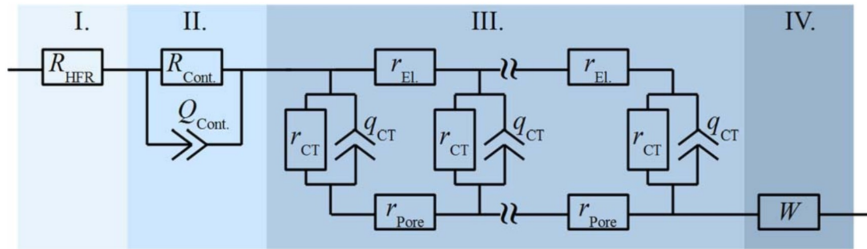


Figure 3.9: Equivalent circuit for porous electrodes; image from "An analysis protocol for three-electrode li-ion battery impedance spectra: Part i. analysis of a high-voltage positive electrode", Journal of The Electrochemical Society 164.7 (2017), A1773-A1783.

and in the follow reported. The model was obtained from the equivalent circuit in figure 3.9. Four physical mechanism are embedded in the model:

- I) high frequency resistance ( $Z_{HFR}$ );
- II) contact resistance between active material and current collector ( $Z_{cont}$ );
- III) ion migration and electron conduction across the thickness of the pores of the electrode ( $Z_{pore}$ )
- IV) Warbutg diffusion element ( $Z_W$ ).

The overall cathode impedance is

$$Z_{cathode} = Z_{HFR} + Z_{cont} + Z_{pore} + Z_W. \quad (3.7)$$

$Z_{HFR}$  is the sum of set up resistance and electrolyte inside the separator:

$$R_{HFR} = R_{setup} + R_{sep}. \quad (3.8)$$

The second mechanism is the contact impedance constituted from a resistance and a capacitance in parallel (simple interface). The capacitance is expressed as a constant phase element which impedance is defined as  $Z = [Q \cdot (i\omega)^a]^{-1}$ . The impedance contribute of the two elements in parallel is given by:

$$Z_{cont} = \frac{R_{cont}}{R_{cont} \cdot Q_{cont} \cdot (i\omega)^a + 1}, \quad (3.9)$$

where  $\omega$  is the angular frequency.

The third block of the equivalent circuit is a transmission line equivalent circuit, composed of incremental elements of the charge transfer resistance ( $r_{CT}$ ), the interfacial double layer capacitance of the cathode ( $q_{CT}$ ), the purely electronic resistance in the electrode ( $r_{el}$ ) and the purely electronic resistance of the electrolyte; see again figure 3.9. The impedance from the general transmission line model is given by:

$$Z_{pore} = Z_{\parallel} + Z^* \frac{1 + 2 \cdot p \cdot s \left[ \sqrt{1 - \tanh(\nu)^2} - 1 \right]}{\tanh(\nu)} \quad (3.10)$$

with

$$Z_{\parallel} = \frac{Z_p \cdot Z_S}{Z_p + Z_S} \quad (3.11)$$

$$Z^* = \sqrt{(Z_p + Z_S) \cdot Z_Q} \quad (3.12)$$

$$p = \frac{Z_p}{Z_p + Z_S} \quad (3.13)$$

$$s = \frac{Z_S}{Z_p + Z_S} \quad (3.14)$$

$$\nu = \sqrt{\frac{Z_p + Z_S}{Z_Q}} \quad (3.15)$$

$$Z_Q = \frac{R_{CT}}{R_{CT} \cdot Q_{CT} \cdot (i\omega)^a + 1}. \quad (3.16)$$

$Z_S, Z_p$  and  $Z_Q$  represent the impedance of the electron conducting solid phase of the electrode, of the ionically conducting pore phase of electrode and of the solid/electrolyte interface surface within the electrode, respectively. These elements are described as electrical resistance throughout the electrode ( $Z_S = R_{el}$ ), by ionic resistance throughout the electrode ( $Z_p = R_{pore}$ ) and by a parallel element of  $R_{CT}$  and  $Q_{CT}$  describing the solid/electrolyte interface surface of the active material in the electrode.

The last part accounts the salt concentration gradients evolving at low frequencies inside the separator. It is represented by a *Warburg element* and its impedance response is described by:

$$Z_W = \frac{W}{\sqrt{\omega}} - i \cdot \frac{W}{\sqrt{\omega}}. \quad (3.17)$$

Theoretically a Warburg element must be placed after a charge transfer resistance to describe the slow solid-state diffusion process inside the active material. In the cited work, this way to use Warburg element is mathematically justified as an element

to describe the liquid concentration gradients inside the separator, because its impedance is considered much larger than the solid-state diffusion.

### 3.3.4 Validation of impedance spectra

Before performing the regression on data, a good approach is to validate them in term of Impedance Spectroscopy criterion exposed in section 2.5.3.

Linearity was verified one time for the system performing two consecutive measures with a voltage amplitude of 5mV and 15mV. The results are perfectly superimposed, therefore the relation is linear or Ohmic, spectra are shown in figure 3.10. With an higher amplitude the signal-to-noise ratio increases and the curve is smoother.

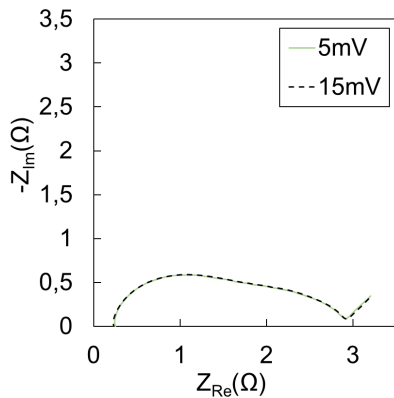


Figure 3.10: cathode impedance spectra of the same cell for two value of stimulus amplitude.

To verify stability and causality criterion an approach taken from the *complex dielectric function* from optics si used that exploit *Kramers-Kroening relations* (KK) [38]. KK relations are bidirectional mathematical relations connecting the real and imaginary parts of any complex funtion that is analytic in the upper half-plane. these relations are often used to calculate the real part from the imaginary part (or vice versa) of response functions in physical systems, because for *stable* systems, *causality* implied the analytical condition, and conversely, analyticity implies causality of the corresponding stable physical system [39]. For a complex function  $f(\omega) = f'(\omega) + jf''(\omega)$  the relation are:

$$f'(\omega) = \frac{1}{\pi} P \int_{-\infty}^{\infty} \frac{f''(\omega')}{\omega' - \omega} d\omega' \quad (3.18)$$

and

$$f''(\omega) = -\frac{1}{\pi} P \int_{-\infty}^{\infty} \frac{f'(\omega')}{\omega' - \omega} d\omega'. \quad (3.19)$$

The direct computation of Kramers-Kronig relations requires a frequency spectrum from zero to infinity. Since an EIS measure is limited to a finite set of frequencies, a different method based on the regression of a model function can be used. If a function, which is analytically *Kramers-Kroening transformable*, can fit data with unbiased and stochastic regression residues, the measure satisfy KK ralation and so the criteria of causality and stability. An example of function that is KK trasformable, is the one that describe the impedance of a circuit composed of an infinite number of *Voigt elements*<sup>8</sup>, see figure 3.11 in series

8: A Voigt element is a resistance with a capacitor in parallel.

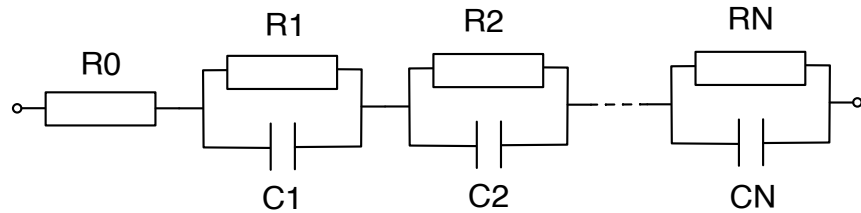


Figure 3.11: Circuit composed with a resistance and an infinite number of Voigt elements in series; it is a Kramers-Kronig transformable circuit.

with a resistance. The impedance of the circuit is given by:

$$Z_{Voigt} = Z_0 + \sum_{i=1}^{\infty} \frac{R_i}{1 + j\omega\tau_i}. \quad (3.20)$$

The validation is more reliable if the number of elements tends to infinity, but a measure is always affected by some stochastic noise which is not included in the model and cannot be fitted. For this reason only a finite number of Voigt elements can be included in the model function. In this work 17 elements were used for the regression, the number is arbitrary and depends on the system. A good practice should be to add one voigt element per time and regress the function until the  $\chi^2$  (standard deviation of the regression) is minimum. Note that the parameter extracted from the regression have absolutely no physical meaning, the process is only a mathematical verification.

Starting parameters were random generated from a 0 to 1 range (because of the non-physical meaning) and the regression was performed several time using the minimum parameters found in the precedent regression step, until convergence. At this point the error residues were evaluated, the points with anomalous bigger error in respect to the others where eliminated because considered biased (and non stochastic).

This procedure eliminates high frequency points, affected by instrumental biases, and low frequency points, affected by a system evolution due the long time needed to acquired them. An example of final results is reported in figure 3.12A.

### 3.3.5 Quality of regression

Two issues affect the overall quality of the regression. First, the validation process removes too many points in the high frequency region and as a consequence the algorithm is no longer

capable to fit the first semicircle and find a reasonable value of the resistance at high frequency ( $R_{HFR}$ ). In this scenario the regression process fits badly the first arc and the arc convoluted with it, see figure 3.12B. The second arc is not much affected. Since the first part of the spectrum remain very similar for all spectra (see discussion in next chapter) it is important to keep it in the fitting to compare the parameter of the minimization between different measures.

The second shortcoming of this approach applied in the work is the *lack* in the model of the convoluted semicircle together with the first arc. Therefore the final fitting (figure 3.12C) is not good enough. This can be also seen in the error residues that are not stochastic at all.

The aim of doing a validation of data is to exclude form regression procedure points that are affected by bias error and can increase the standard deviation of the regression. Since the model fail itself to fit correctly data, validation becomes unnecessary and regressions were performed directly on full data sets. For the same reason was not made the relatively time-consuming effort to implement computation of covariance matrices in the code. Resulted parameters are intended to be evaluated as qualitative.

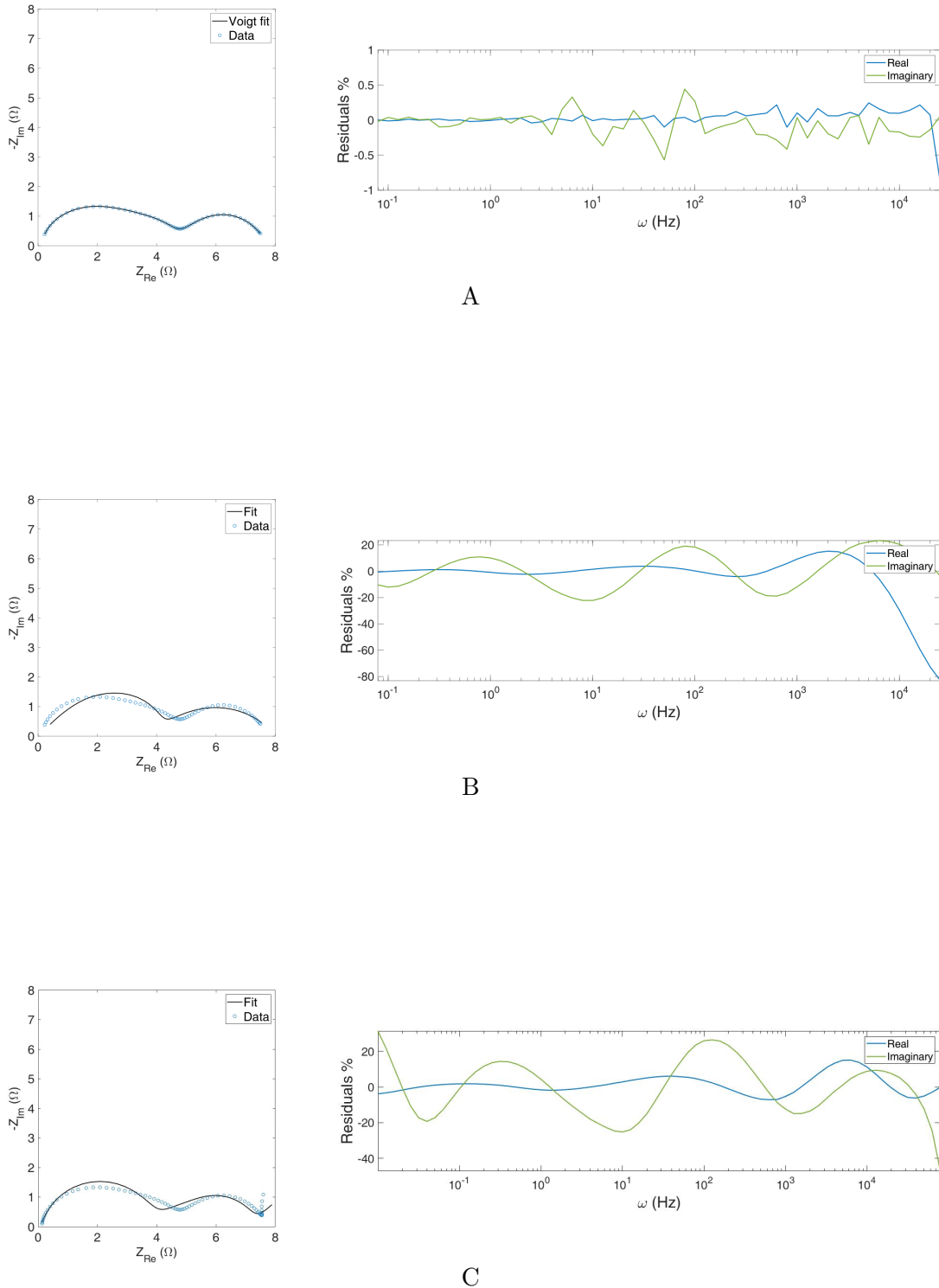


Figure 3.12: Complex non-linear regression and their residues for: A - validation through Voigt circuit; B - regression of theoretical function over validated data; C - regression of theoretical function over non-validated data



# 4 | Results and comments

In this chapter are discussed results from four pouch cells. One of them was cycled in a two-electrode configuration and the others in three-electrode configuration. Impedance of both electrodes and full cell were measured, presented here and compared. The focus of the work was the NMC622 cathode because for graphite anode a wide literature is already present. The effect on cell design and pressure condition on cathode impedance and its dependence on temperature were described. Names of cells built and tests performed for each one are reported in table 4.1.

## 4.1 Cycling performances of cells

From galvanostatic cyclation, was found that pressure plays an important role on the anode potential. For a cell without a pressure applied, during discharge the counter electrode potential tends to drops under 0V vs  $Li/Li^+$  activating the lithium deposition reaction. In figure 4.1 is reported the potential profile of the anode for a C-rate of C/10 and it remains below 0V for almost two hours. To preserve electrodes from lithium plating, a limit ad 0V to the cathode was used, but this limited the charge of the battery. In fact, the working electrode potential stops between 3.8V and 4.1V vs  $Li/Li^+$ .

With a high pressure applied cells charged correctly at current until a C-rate of C/4, but a problem was found in the discharge step. The potential of counter electrode get to high, over the imposed limit of 2V and the cell cannot discharge completely. The working electrode stops around 3.7-3.8V. Therefore anode in the batteries built was not optimized and . Furthermore the trend of electrode resistances, estimated through impedance spectroscopy as a function of number of complete cycles<sup>10</sup>, were not obtained.

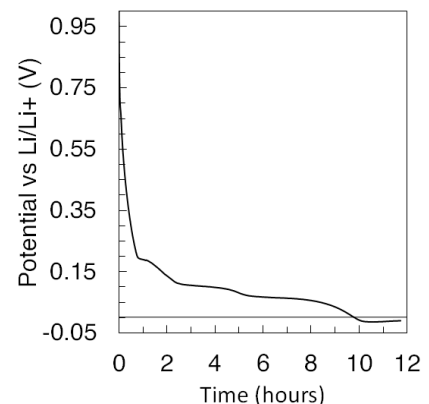


Figure 4.1: Counter electrode potential in pouch cells under the pressure of two paperclips, first cycle at C/10.

10: It is a way to quantify aging of the electrode and attribute the sources.

Name	Tests
Pouch 1	PEIS after assembling A/C/F 5 cycles C/20 140 cycles C/2 (Galavanostatic with potentiostatic in charge and dischahrge C/30) PEIS A/C/F at SOC 0% cycles 5,6,11,16 and 34 PEIS A/C/F at SOC 100% cycles 4 and 16 (all $T_{room}$ and $P_{atm}$ )
Pouch 2	PEIS after assembling C 2 cycles C/20 22 cycles C/2 PEIS A/C/F SOC 0% cycles 2 and 3 PEIS C at SOC 100%, 10% and 0% cycles 4-24 (all $T_{room}$ and $P_{atm}$ )
Pouch 3	PEIS after assembling A/C/F 5 cycles C/10 PEIS A/C/F SOC 0% changing pressure PEIS A/C/F SOC 50% changing temperature
Pouch 4	PEIS after assembling A/C/F 1 cycle C/20 10 cycles C/4 PEIS C at SOC 100% and 10% cycles 2-11 (all $T_{room}$ and under two level if pressure)

Table 4.1: Test performed on the pouch cell discussed in this chapter; The letters A, C and F stand for anode, cathode and full cell to indicate which spectra was collected.

## 4.2 Shapes of impedance spectra after cell assembling

After the assemble of a cell, before any current applied to the battery, the shapes of electrodes impedance are very different from what is observed during operation (discussed in next section). Examples of electrodes spectra are reported in figure 4.3. At this stage the anode is completely delitiated and there is no SEI formed. The low frequency region is usually attributed to solid-state diffusive phenomena [28] that here is missing and a capacitance behavior is observed. Cathode impedance spectrum shows two convoluted depressed semicircles at higher frequencies,

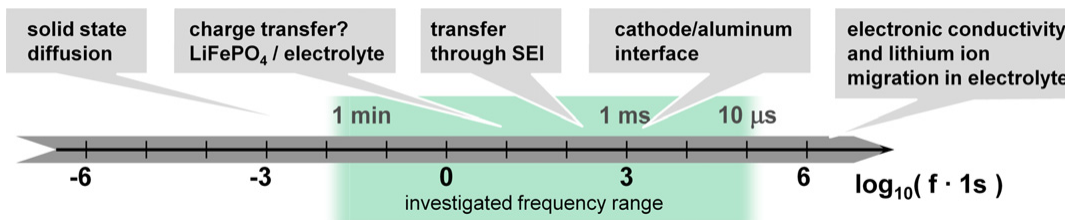


Figure 4.2: Time scale of typical processes inside LiFePO<sub>4</sub> cathode; similar for all porous electrodes; image from Jan Philipp Schmidt et al. "Studies on LiFePO<sub>4</sub> as cathode material using impedance spectroscopy". In: *Journal of Power Sources* 196.12 (2011), pp. 5342–5348.

a linear feature with an angle of ca. 60° and the capacitance behavior at medium-low frequencies. The anode shows one small semicircles, the linear feature with an angle of ca. 30° and then the capacitance part.

Impedance spectra are very challenging to interpret, but many mechanisms can overlap and the results is dependent on electrode material and cell geometry. Typical time scales for processes that occur in a porous electrode material, are reported in figure 4.2. Starting from here, each mechanism is attributed to frequency intervals of the various features in the spectrum in study.

In figure 4.4, impedance spectra for two pouch cells and a Swagelok cell are reported to be compared. Pouch 4 is under a pressure of 3.2 KPa and the shapes and resistance value are very similar to Pouch 1 which is not under pressure. For the Swagelok, resistance is higher because the area is 12 time smaller, but normalized values are comparable. Furthermore the intercept i much higher due to the ticker separator.

At this stage the quality of the reference electrode to separate electrodes impedance is evaluated comparing the full cell spectrum with the sum of cathode and anode spectra. Was found that this separation is very good with a discrepancy of the sum from the full cell of less than 2.5%. In some measurements, points at high frequencies (usually first 5 points) in single electrode spectra contain some instrumental error and were removed.

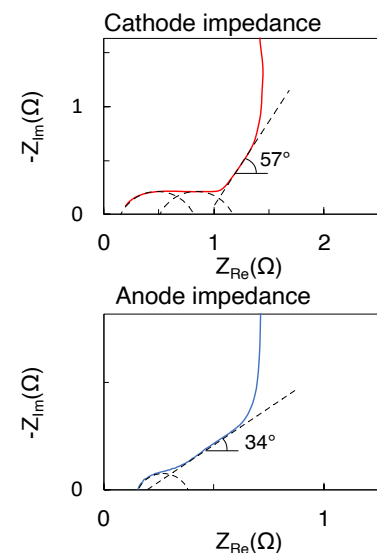


Figure 4.3: Shapes of cathode and anode spectra after assembling.

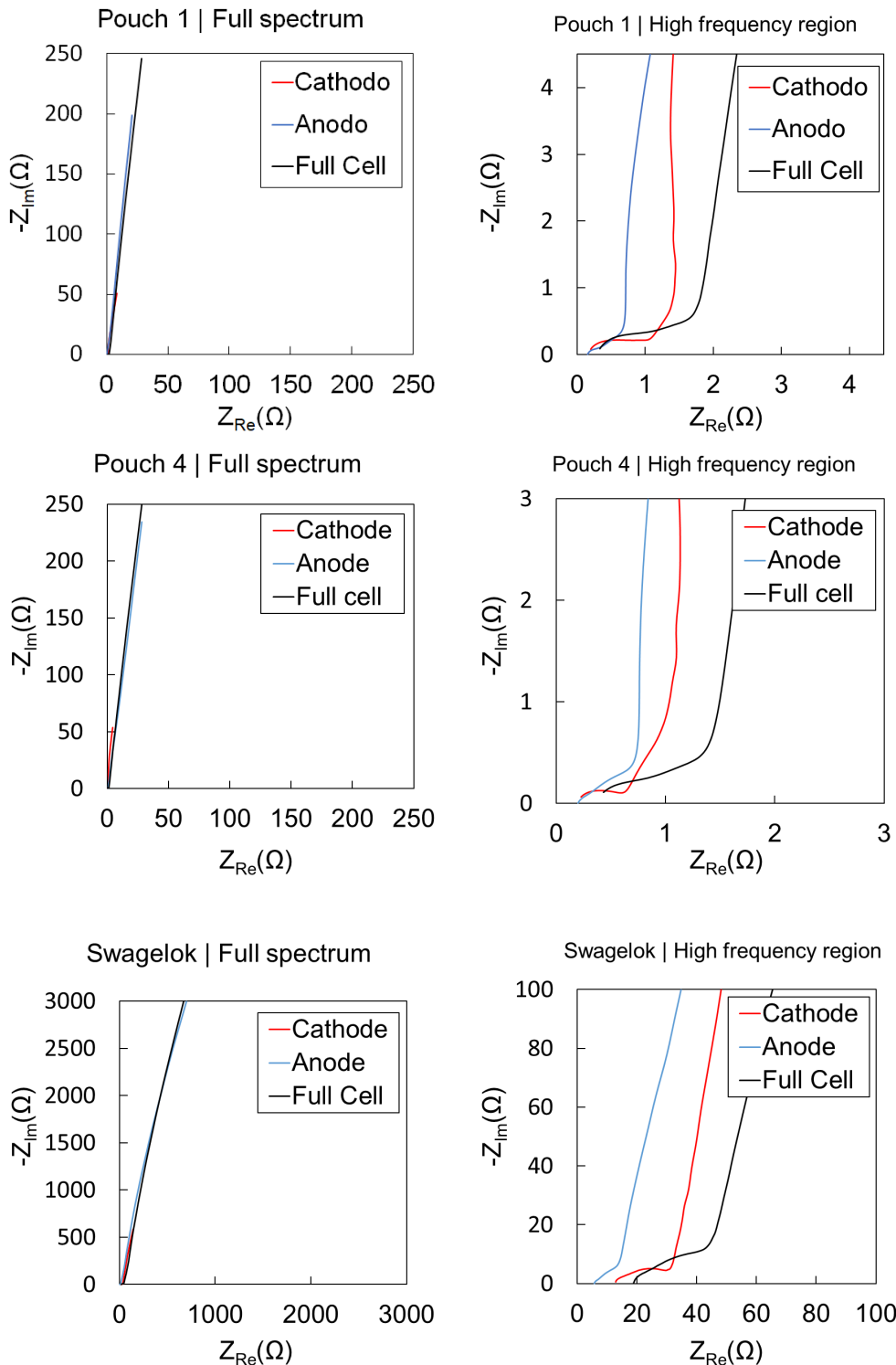


Figure 4.4: Impedance spectra after assembly for two pouch cells (Pouch 1 without pressure and Pouch 4 with pressure) and a Swagelok cell which is always in pressure.

### 4.3 Shapes of impedance spectra after a current flow

Impedance spectra were mainly acquired in the *discharge state*, only because it is easier to do during cycling of the battery. Despite the change in state of charge, spectra shapes remain very similar to the one shown in figure 4.5 and only resistance values change. The set-up is capable to separate the electrode behavior in two defined semicircle in both cathode and anode side, this shape is typical of the *porous electrode* [28],[41],[31] which distinctive elements are: the *intercept* with the abscissa corresponding to the resistance of the electrolyte in the separator; a *first semicircle* corresponding to the polarization of the double layer; a *second semicircle* related to the charge transfer process; a  $\sim 45^\circ$  feature which represent the solid state diffusion into SEI. Graphite anodes analyzed in this work present a small semicircle, a second bigger semicircle and finally the diffusive tail. For both electrode is present another convoluted semicircle that is not described i literature.

For NMC622 cathodes studied in this work, was found that the first semicircle is convoluted with another small semicircle, not expected in the models described in literature. Another mechanism is highlighted in this set-up, it may be a two-step charge transfer phenomena [trocoli2018phase] but it an in dept investigation is needed.

### 4.4 Repeatability of EIS measure

With the aim of use Electrochemical Impedance Spectroscopy to get a unique footprint of the electrodes, it is important to remove all external sources of alteration. Cell tested in this work was changed in position over the instrument table because of the availability of instrument channel equipped with an Frequency Response Analyzer. The moving of cell by hands modify in some way the shape of the plastic case of the battery and that produced repercussions on the spectra. As an example of this issue the impedance of pouch 1 during cycling is reported in figure 4.6. Points up to 2-3Hz of all the curves are quite similar but for lower frequencies spectra are noticeably different. High frequencies spectrum represent the response of interface that does note change significantly. The lower part of the spectrum exhibits the response of diffusive phenomena and phase shifts which can largely depends on the condition of the separator.

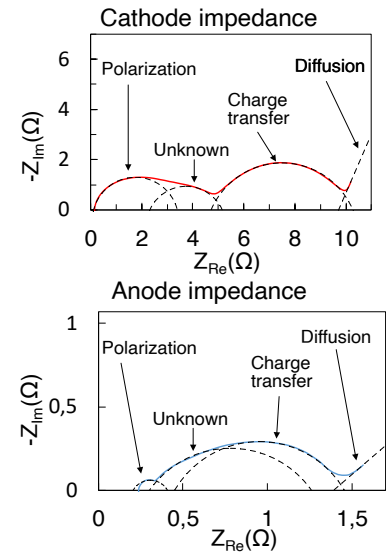


Figure 4.5: Shapes of cathode and anode spectra.

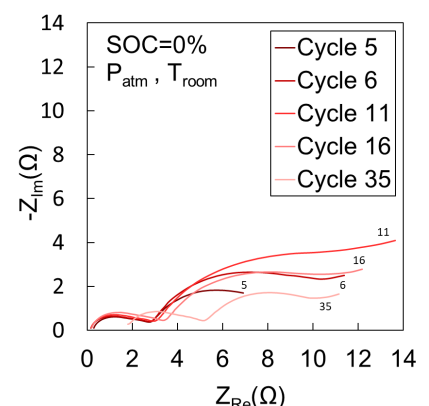


Figure 4.6: Cathode impedance at different number of cycle for Pouch 1.

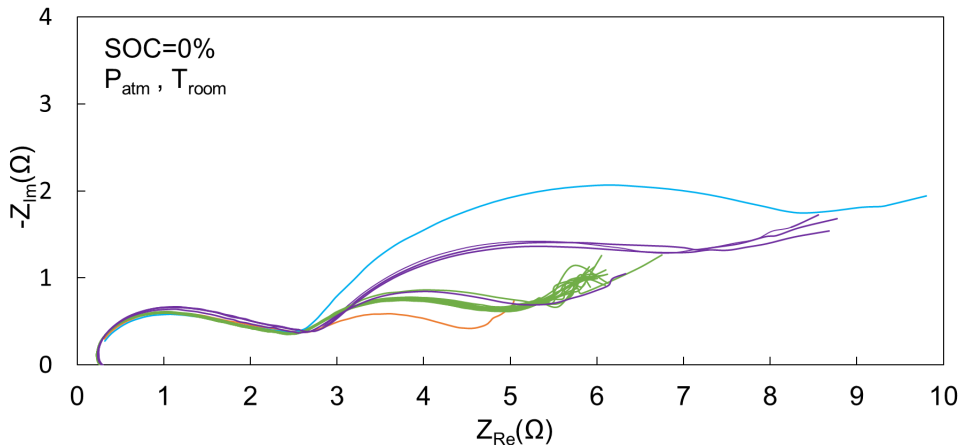


Figure 4.7: Cathode impedance of Pouch 2 during cycles; colors represents different sets of measures, between two sets the cell was mechanically altered moving it and swapping crocodile clips.

It is clear that a mechanical alteration of the case produce a change in position or areas of contact for the element in the battery stack. In some cases a rigid translation of spectra are found. The shapes and resistance values remain the same but it is like an additive resistance is placed at the beginning of the circuit, maybe due to a bad connection of crocodile clip during the swapping. An example is the cycle 35 of figure 4.6.

As a counter-example the impedance of Pouch 2, measured during cycling without moving the cell, is reported in figure 4.7. Spectra depicted in the same color behave to the same set of impedance measures in which no mechanical alteration took place. The cell was kept in the same three-electrodes configuration for cycling and impedance measure. After the acquisition of a set of spectra, crocodile clips were interchanged to acquire anode impedance and this produced a change in shape of the successive set of cathode measures. The first arc at high frequency is still unchanged from different sets.

As expected the impedance of two consecutive cycles must be very similar when no external parameters affect them. In fact, aging process require at least some tens of cycle for an appreciable effect [42], therefore it is expected to have identical or very similar impedance spectra in successive measures.

When no external contribution alters the cell impedance, it is possible to compare two cathode impedance of two different

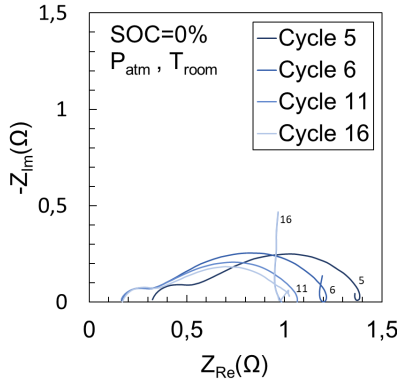


Figure 4.9: Anode impedance of Pouch 1 at different number of cycles.

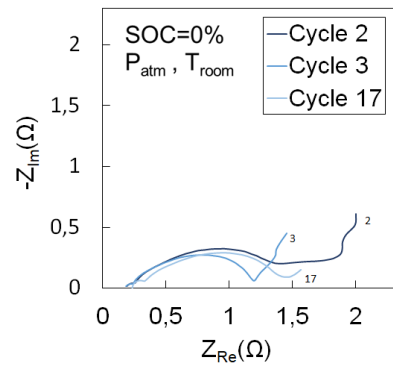


Figure 4.10: Anode impedance of Pouch 2 at different number of cycles.

battery as reported in figure 4.8. It is a promising sing that optimizing the cell condition can produce a reproducible method.

On the anode side the same problem of mechanical sensitivity occurs and it was found to be more prone to show loops and instrumental artifacts, see figures 4.9 and 4.10. The first points, up to 100Hz, are comparable between different measurement.

## 4.5 Effect of the pressure on impedance spectra

Pressure gives an important contribution to cathode impedance. In figure 4.11 are reported two spectra for the same pouch cell with and without an external pressure applied. A small pressure of 2.7KPa is sufficient to reduce cell resistance a lot. All resistances are reduces: both semicircles and the high frequency intercept. The reason of the behavior is attributed to a better electrodes/separator contact which distribute the line of current to a wider area reducing the resistance (input voltage is constant).

## 4.6 Stationarity of batteries

With the term *stationarity* is meant the stability of system parameters between two different measures. The data presented in the follow, were taken to evaluate the stochastic error brought

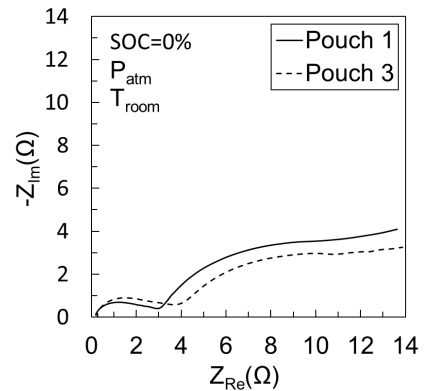


Figure 4.8: Cathode impedance of Pouch 1 and Pouch 3, at fifth and second cycle respectively.

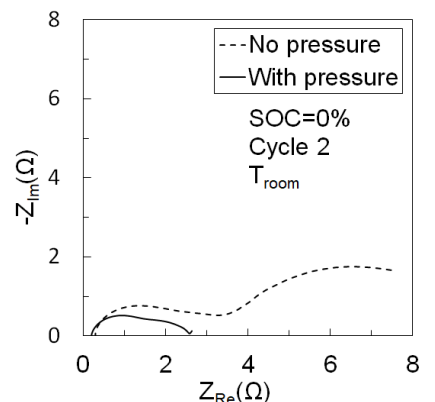


Figure 4.11: Cathode impedance of Pouch 3 under different pressure condition.

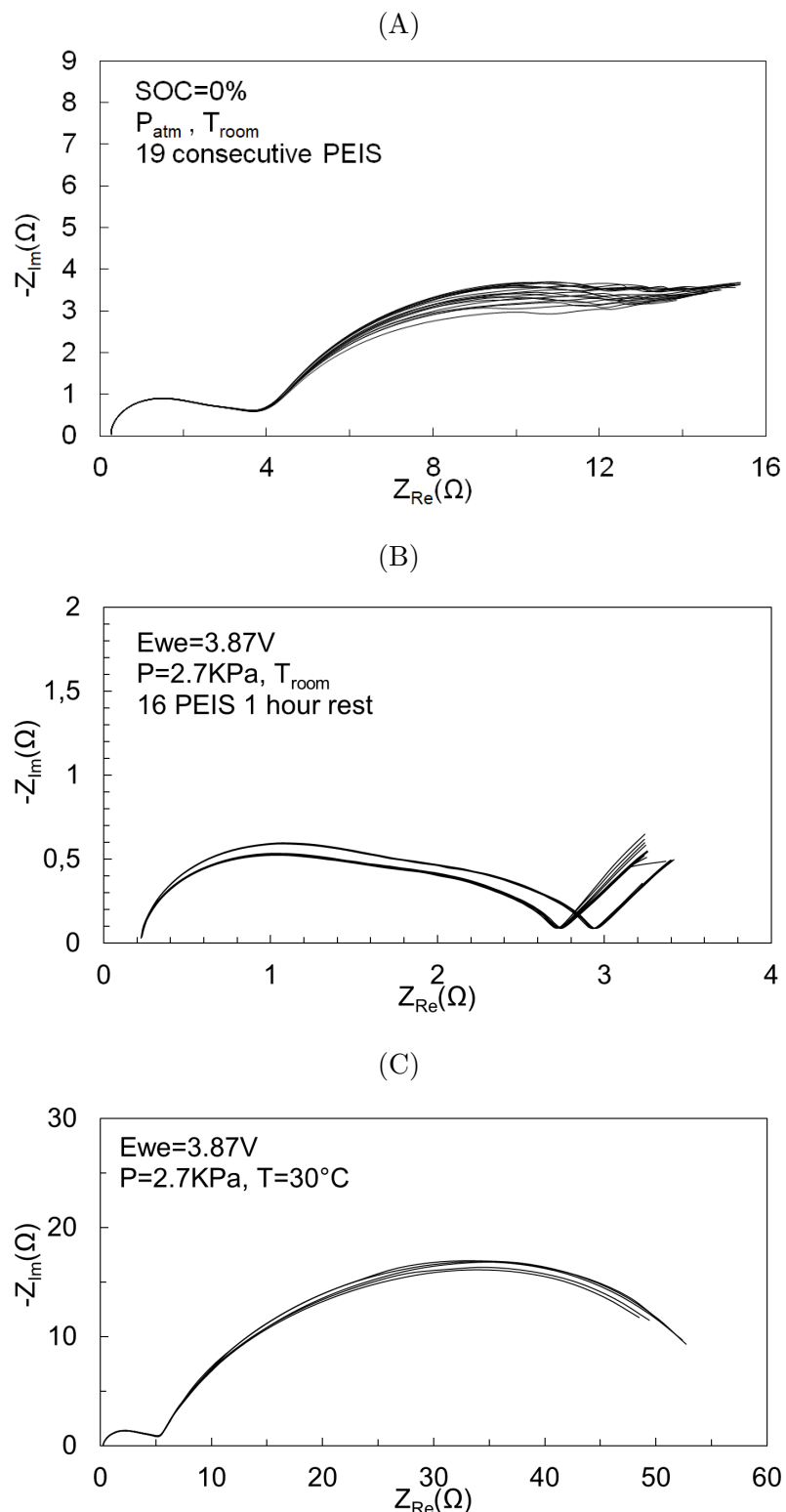


Figure 4.12: Impedance spectra after assembly for two pouch cells (Pouch 1 without pressure and Pouch 4 with pressure) and a Swagelok cell which is always in pressure.

by the set-up for each frequency. A frequency dependent stochastic error function is a better weighting function for non-linear regression [38]. As described in previous chapter the theoretical function was not adequate for the system in study, so a fine tuning of the regression procedure is pointless. This data remains useful to comment the role of temperature and pressure on the repeatability of an Impedance Spectroscopy Measure.

To evaluate the stationarity of a cell, different impedance spectra were measured consecutively without changing external conditions. Three tests were performed and presented in figure 4.12. Measures in figure 4.12A show that without pressure and at room temperature the second semicircle is evolving in time (19 hours in total) and the cell was kept in OCV for two days before the test.

With a pressure applied, see figure 4.12B, the system is more stable but after few cycles there was a significant variation in resistance, attributed to an autonomous mechanical relaxation of the battery case.

Moving the cell in the laboratory oven, brought another mechanical alteration, see figure 4.12C. The pressure clearly was not reestablished correctly and the resistance of the cell is very high. Nonetheless the controlled temperature keeps the system more stable.

Figure 4.12A represents the completely discharged battery, while B and C are referred to an higher state of charge because the cell under pressure was no longer able to discharge. The effect of the state of charge on the stability of the system was not entirely investigated.

## 4.7 Effect of the temperature on impedance spectra

### 4.7.1 Qualitative analysis of spectra

To reveal the influence of temperature on the impedance of the system, four measures were performed at 30°C, 40°C, 50°C and 60°C, results and reported in figure 4.13 (next page). The set-up is capable to separate well two depressed semicircles, one at

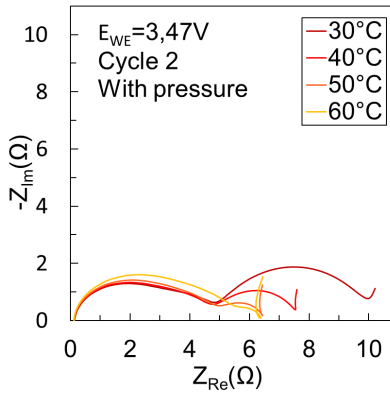


Figure 4.13: Cathode impedance of Pouch 3 for different temperatures.

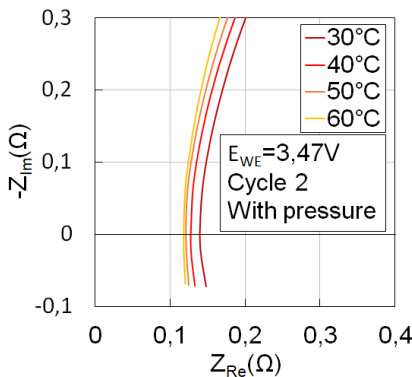


Figure 4.14: High frequency region of cathode impedance of Pouch 3 for different temperatures.

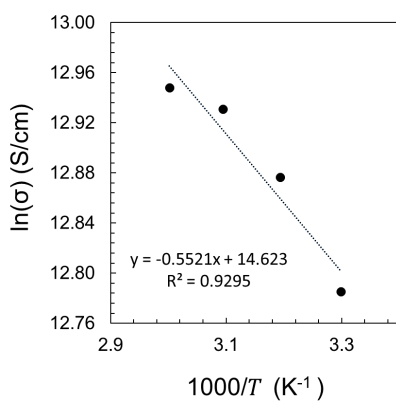


Figure 4.15: High frequency resistances in Arrhenius plot; dotted line is the linear regression, the equation and  $R^2$  are reported in the chart.

lower frequency that decrease with temperature and another at higher frequency that increase slightly with temperature. The diffusive tail have too little points to study its behavior, so it will not be discussed. The high frequency intercept decreases with temperature and to see this a chart enlarged in the high frequency area is reported in figure 4.14.

Let start the discussion with the intercept at high frequency. The viscosity  $\eta$  of a liquid reduces with the temperature [43] and the ionic mobility  $\mu$  increases because the inversely proportionality. *Ionic conductivity*  $\sigma$  is directly proportional to ionic mobility. The conductivity of a thermally activated ion-transport process is usually described by a simple Arrhenius expression [44], [45]:

$$\sigma(T) = \sigma_0 e^{-E_a/k_b T}, \quad (4.1)$$

where  $\sigma$  is the specific conductivity,  $\sigma_0$  is the  $E_a$  is the energy activation of the diffusion process,  $k_b$  is the Boltzmann constant ( $8.62 \times 10^{-5} \text{ eV} \cdot \text{K}^{-1}$ ) and  $T$  is the temperature. Plotting experimental data in an Arrhenius Plot, figure 4.15, the activation energy could be found from the slope of the linear regression of data points. The estimate value for energy is  $4.76 \times 10^{-2} \text{ eV}$ . This value is lower, but the same order of magnitude of the activation energy of electrolyte in porous electrodes of 0.2-0.3 eV as reported by Schmidt et al. [40]. The high frequency resistance have several physics reasons. It is caused buy the limited electronic and ionic conductivities of all cell components.

From figure 4.13 is noticeable that *total resistivity*, composed by electrolyte intercept and the two depressed semicircles, reduces with temperature in fact all chemical reactions are thermally activated. The second semicircle reduces with temperature but the first one increases. First semicircle is linked to interface processes and the second with diffusion and phase change. Charge transfer is strongly dependent on the temperature because the diffusivity of  $\text{Li}^+$  inside SEI is temperature-dependent [46]. Using the integrate circular fit of EC-Lab software, resistances of second semicircle for each spectra were extracted and reported in an Arrhenius Plot, in figure 4.16, to evaluate the activation energy. A similar equation to 4.1 can be written for resistivity:

$$\frac{1}{R_2} = A e^{-E_a/k_b T}, \quad (4.2)$$

where  $R_2$  is the resistivity of second semicircle and  $A$  the prefactor of exponential. The value of the prefactor is not important because it only leads to a rigid translation of the line. The linear

Temperature (°C)	$R_{HFR}$ ( $\Omega$ )	$R_{cont}$ ( $\Omega$ )	$R_{CT}$ ( $\Omega$ )	$R_{tot}$ ( $\Omega$ )
30	0.140	2.924	5.525	9.98
40	0.128	3.098	3.105	7.54
50	0.121	3.244	1.714	6.43
60	0.119	3.799	1.181	6.38

Table 4.2: Resistances obtained from visual analysis and EC-Lab circular fit.

regression of data point have a good  $R^2$  of 0.994 and from the slope an activation energy of 0.45eV is obtained, very close to the medium value of 0.6eV estimated by Keefe et al. [46] and of 0.66eV by Schmidt et al. [40].

The first semicircle is constant for spectra measured from 30 to 50°C and change for 60°C, see figure 4.13. This part of the spectrum is associated with polarization and interfaces phenomena and there is not any description of temperature dependency in literature. The result at 60°can be connected to a *degradation phenomena*, like for example dissolution of nickel, a known common issue of high-nickel (>0,5) NMCs that is thermally dependent [47].

### 4.7.2 Analysis of regression results

Values of circuits elements extracted with the complex non-linear regression of data can be compared with the qualitative discussion in previous section. The model proposed by Landesfeind, Pritzl, and Gasteiger [35] and used in this work, is not sufficient to describe the system because the convoluted semicircle with the first one is not expected. A better function it is needed to be developed but something interesting can still be said with this rough regression.

To understand the issue with fitting, an example of fitting is presented in figure 4.18A. In the high frequency region there are a lot of points and the minimization algorithm use a well defined and low-depressed semicircle to fit this area. The intercept value is 20-30% less of the real value, and this is because it is very small and the algorithm tries to enlarge the semicircle to fit also lower frequency points. As frequency decrease the regression loose accuracy because of the convoluted semicircle and the second semicircle, associated to charge transfer starts in advance; to fit the most number of points the algorithm widens

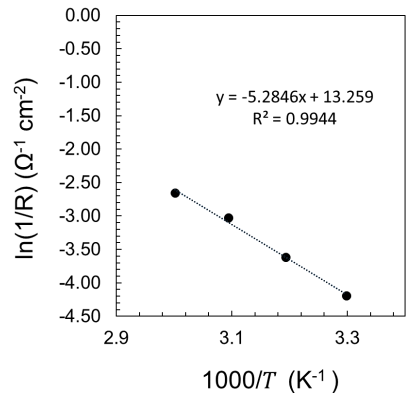


Figure 4.16: Estimated resistances from the second arc of spectra in figure 4.13, reported in Arrhenius plot; dotted line is the linear regression, the equation and  $R^2$  are reported in the chart.

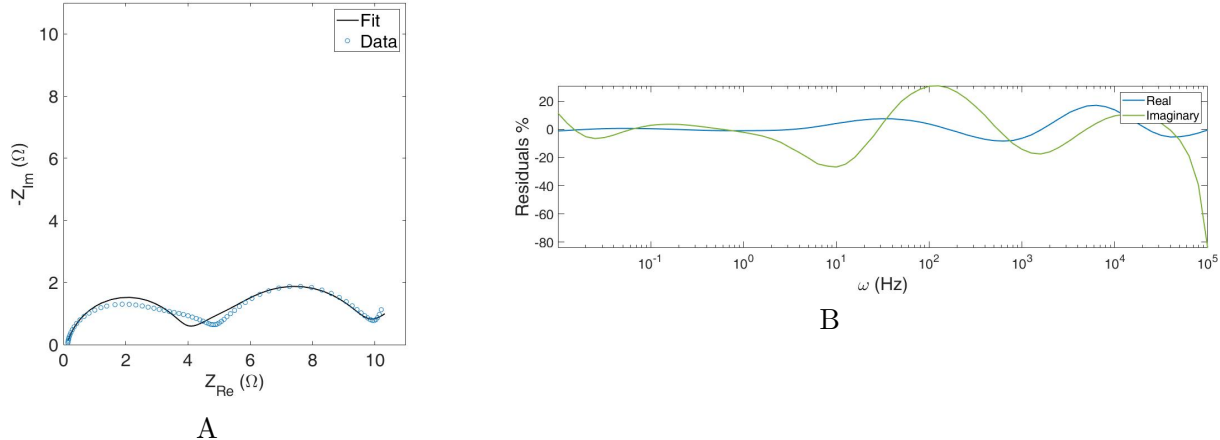


Figure 4.18: Complex non-linear regression of cathode impedance for Pouch 3 at 30°C; A- fitting of theoretical function over data , B- regression residues as a function of frequency.

the semicircle. The low frequency tail contains few points and the parameters quality will not be discussed. The poor quality of data is represented from the "wavy" trend of error residues in figure 4.18B.

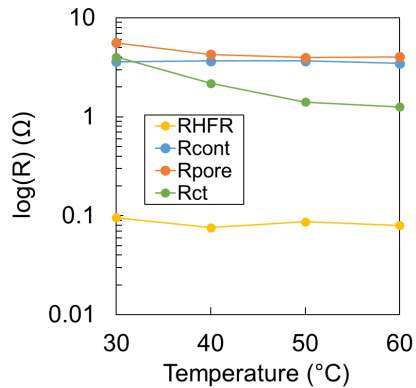


Figure 4.17: Trends of system resistances with temperature; values are obtained by complex non linear regression, full parameters are presented in table 4.3. Resistances are reported in logarithmic scale.

Minimum parameters from regression of data are reported in table 4.3 for all four temperature. The resistances values in respect to temperature are depicted in figure 4.17. This results are similar to what found in the qualitative analysis in term of value and trend with temperature, but they need to be taken as a qualitative insight of the regression procedure, since the error was not computed. The high frequency resistance remains constant instead of decreases because its value of decrement is very small and the error of fitting a lot bigger (as can be visually estimated). Contact resistance remain constant around 3.7 Ω for temperature between 30 to 50°C and is a bit lower for 60°, 3.45Ω. Pore and charge transfer resistance reduce with temperature as expected. The points at 50 and 60°for charge transfer resistance are higher than the real ones because the algorithm fails to fit small semicircle with few points and instead tries to fit the convoluted semicircle as a charge transfer process. Resistance values obtained from EC-Lab circular fit are reported in table 4.2. All fitted spectra and their error residues are reported in appendix C. Pore resistance is embedded the second semicircle and it cannot be evaluated in the qualitative analysis.

<b>T=30°C</b>		<b>T=40°C</b>	
<b>Parameter</b>	<b>Value</b>	<b>Parameter</b>	<b>Value</b>
R <sub>HFR</sub>	9.57 10 <sup>-2</sup> Ω	R <sub>HFR</sub>	7.58 10 <sup>-2</sup> Ω
R <sub>cont</sub>	3.60 Ω	R <sub>cont</sub>	3.66 Ω
Q <sub>cont</sub>	4.80 10 <sup>-4</sup> μF· s <sup>a<sub>cont</sub>-1</sup>	Q <sub>cont</sub>	5.09 10 <sup>-4</sup> μF· s <sup>a<sub>cont</sub>-1</sup>
a <sub>cont</sub>	0.855	a <sub>cont</sub>	0.847
R <sub>pore</sub>	5.61 Ω	R <sub>pore</sub>	4.28 Ω
R <sub>el</sub>	3.96 10 <sup>-8</sup> Ω	R <sub>el</sub>	1.42 10 <sup>-7</sup> Ω
R <sub>CT</sub>	4.02 Ω	R <sub>CT</sub>	2.18 Ω
Q <sub>CT</sub>	4.02 μF· s <sup>a<sub>CT</sub>-1</sup>	Q <sub>CT</sub>	3.50 10 <sup>-1</sup> μF· s <sup>a<sub>CT</sub>-1</sup>
a <sub>CT</sub>	0.876	a <sub>CT</sub>	0.851
W	8.90 10 <sup>-2</sup> Ω/√s	W	7.10 10 <sup>-2</sup> Ω/√s
χ <sup>2</sup>	7.61 10 <sup>-3</sup>	χ <sup>2</sup>	5.39 10 <sup>-3</sup>

<b>T=50°C</b>		<b>T=60°C</b>	
<b>Parameter</b>	<b>Value</b>	<b>Parameter</b>	<b>Value</b>
R <sub>HFR</sub>	8.67 10 <sup>-2</sup> Ω	R <sub>HFR</sub>	8.00 10 <sup>-2</sup> Ω
R <sub>cont</sub>	3.68 Ω	R <sub>cont</sub>	3.47 Ω
Q <sub>cont</sub>	3.68 10 <sup>-4</sup> μF· s <sup>a<sub>cont</sub>-1</sup>	Q <sub>cont</sub>	2.40 10 <sup>-4</sup> μF· s <sup>a<sub>cont</sub>-1</sup>
a <sub>cont</sub>	0.886	a <sub>cont</sub>	0.931
R <sub>pore</sub>	3.71 Ω	R <sub>pore</sub>	4.04 Ω
R <sub>el</sub>	3.71 10 <sup>-9</sup> Ω	R <sub>el</sub>	1.65 10 <sup>-6</sup> Ω
R <sub>CT</sub>	1.41 Ω	R <sub>CT</sub>	1.26 Ω
Q <sub>CT</sub>	0.220 μF· s <sup>a<sub>CT</sub>-1</sup>	Q <sub>CT</sub>	2.46 10 <sup>-2</sup> μF· s <sup>a<sub>CT</sub>-1</sup>
a <sub>CT</sub>	0.910	a <sub>CT</sub>	1.00
W	5.23 10 <sup>-5</sup> Ω/√s	W	0.153 Ω/√s
χ <sup>2</sup>	9.17 10 <sup>-3</sup>	χ <sup>2</sup>	5.30 10 <sup>-3</sup>

Table 4.3: Minimized parameters for fitting of Pouch 3 cathode impedance at different temperatures.

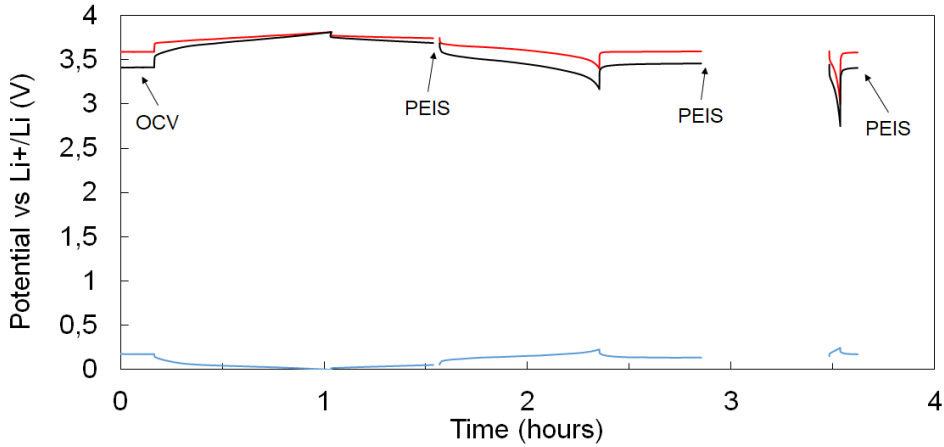


Figure 4.20: Three-electrode galvanostatic cycle 22 of Pouch 2; brakes in line correspond to PEIS measures, the first one is shorter because it is up to 100 KHz.

## 4.8 Effect of the state of charge on impedance spectra

### 4.8.1 Qualitative analysis of spectra

It is known that total cell resistivity is lower at high state of charge [28]. To investigate this effect on cathode impedance, during the cycling of Pouch 2, measures at three different potentials were performed. One measure was performed at high state of charge, at the maximum potential the working electrode can reach before the anode cut-off stops the charge. This is around 3.7-3.8V for Pouch 2 in cycles 4-17. A second measure was conducted at 3.4V which is ca. 10% of the charge left on the anode (in discharge) and the third one was performed at 3V for working electrode or 0% of charge left; see figure 4.20. The above value of potentials are referred to the potential during cycling at a C-rate of C/4. In the following, is analyzed the set of three spectra for cycle 22, reported in 4.19. The potentials at OCV (i.e. after 30 minutes from galvanostatic stop) for working electrode are 3.75, 3.60 and 3.58 and they will be referred as high SOC, medium SOC and low SOC for simplicity. These values are very close together but the impedance spectra are considerably different. At the highest potential the capacity is 15mAh that is the 42% of the theoretical capacity. Therefore the states of charge are roughly 40, 10 and 0%.

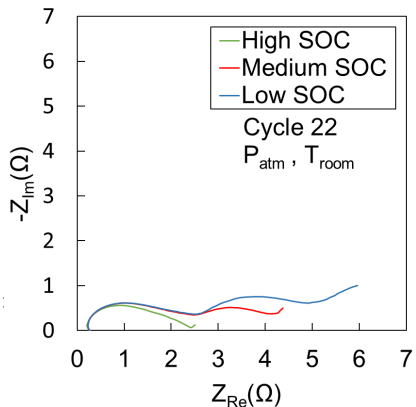


Figure 4.19: Cathode impedance for Pouch 2 at different state of charge.

The high frequency intercept of the spectra is independent

SOC	$R_{HFR}$ ( $\Omega$ )	$R_{cont}$ ( $\Omega$ )	$R_{CT}$ ( $\Omega$ )
High	0.204	1.282	-
Medium	0.210	1.397	2.48
Low	0.211	1.411	3.25

Table 4.4: Resistances values extracted from EC-Lab circular fit for Pouch 2 cathode resistance at cycle 22 and different state of charge.

from the state of charge but it suffers an artifact for highest frequency points that produces a loop toward high resistance value, see figure 4.21. A more correct value was obtained as intercept of EC-Lab circular fit of the first arc of the spectra, reported in table 4.4 together with other value extracted in the same way. The mean value of the three  $R_{HFR}$  was used to calculate an ionic conductivity of  $0.80\text{mS}/\text{cm}$  which is almost an order smaller than the pure electrolyte ( $6.27\text{mS}/\text{cm}$  declared from the producer) that is correct according to literature [21].

The high SOC spectrum have less point because the impedance was measure until 100KHz and the second semicircle is missing. At high state of charge the potential is less stable and a shorter measure was preferred, see figure 4.20 for detail on measure and potentials. Since the state of charge is only up to 40% no other insight can be taken on the behavior of the cell in respect of state of charge.

For Pouch 1 (cycled in two-electrode configuration) a measure of the cathode impedance at a completely charged state is available. In its measurement configuration the potential of working electrodes is not known but for sure is closer to 100% than in the case of Pouch 2 (cut-off EWE-ECE=4.3V vs  $\text{Li}/\text{Li}^+$ ). The result is presented in figure 4.22. The figure shows that at high state of charge both semicircle shrinks, thus both interfaces and diffusion phenomena are dependent on the concentration of lithium in the cathode.

## 4.9 Electrochemical Impedance Spectroscopy in Swagelok cell

Impedance Spectroscopy was performed in a Swagelock type cell to verify if the resulting spectrum has a dependency on the cell geometry. Swagelok electrode are only  $1,13\text{ cm}^2$  and the common separator used is glass fiber with a great excess of electrolyte to

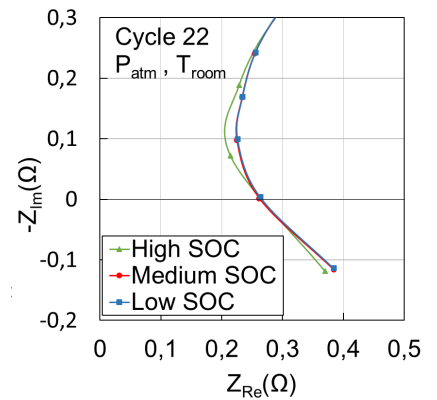


Figure 4.21: High frequency region of impedance spectrum of cathode for Pouch 2 at different state of charge.

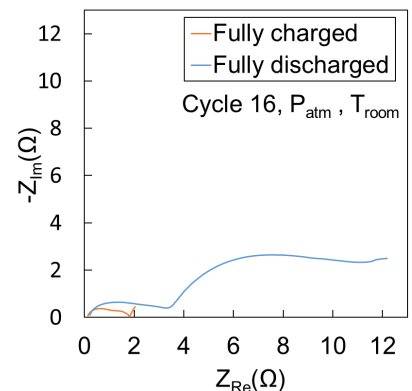


Figure 4.22: Pouch 1 cathode impedance fully charged and fully discharge at cycle 16.

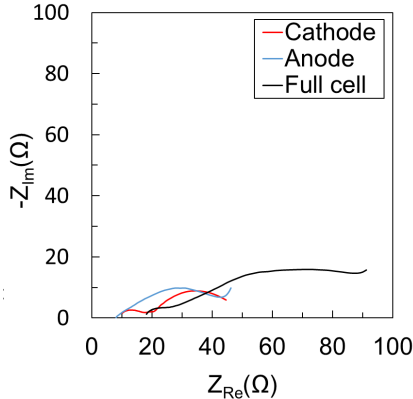


Figure 4.23: Impedance spectra for a Swagelok cell.

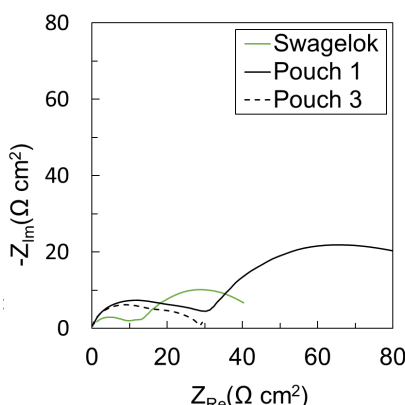


Figure 4.24: Cathode impedance spectra of a Swagelok cell, Pouch 1 that is whiteout pressure and Pouch 3 that is under pressure; data are multiplied by respective areas and the intercept resistance is subtracted.

keep it wet. The impedance for single electrodes and full cell is reported in figure 4.23. More interesting is figure 4.24 where the impedance of the Swagelok cell is compared with pouch cells with and without the pressure. Unfortunately the result, in term of shape, is different in respect to both pouch cells. The order of magnitude is the same of pouch cell and the shape is similar to pouch cell under pressure. The discrepancy was attributed to the different area. Even small defects, that cause a local high resistivity current path, weight a lot in the Swagelok with an area of  $1.13\text{cm}^2$  compared to  $12\text{cm}^2$  of the pouch.

Swagelok cells are easy and fast to assemble, electrodes are well pressed together and the cycling performance are satisfy. However there are a lot of disadvantages. First of all the glass fiber is a different interface than poly ethylene used in real commercial batteries, the signal-to-noise ratio is grater for the higher distances of the electrodes and they are very prone to dry out because of the difficulty to perfectly screw the fixing nuts without damaging the battery stack between pistons.

## 4.10 Visual inspection of post-mortem cells

### 4.10.1 Lithium reference electrode

A lot of insights can be taken with a visual inspection of the components of the cell after testing, especially connecting them with electrochemical test results. First thing it was checked was the state of lithium reference electrode. In figure 4.25A is reported a photograph of the reference electrode of Pouch 1 after 150 cycles. Reference electrodes from cell that had cycled present a strong alteration of lithium. The metal turns into a dark, spongy and soft aggregate. In this state it can works to separate impedance electrodes contributes, but its potential can be significantly different than metallic lithium and any three-electrodes cyclation becomes uncontrolled. In figure 4.25B can be seen a lithium reference of a non tested cell because of a fault just after assembly. The lithium surface has its typical shiny metallic look. The electrode was kept inside the cell for two month, therefore the degradation is not due to the electrolyte exposition but to the small current that the potentiostat supply to measure the polarization. Reference electrodes based on metallic lithium are very easy to prepare and insert into the

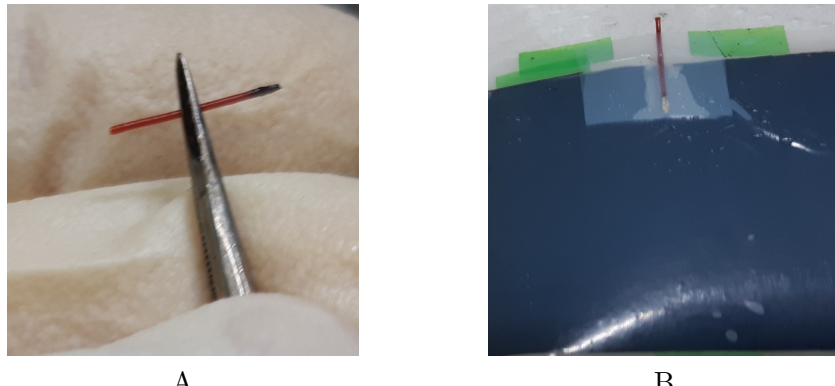


Figure 4.25: Lithium reference electrode of two pouch cells, A is from a cell that performed galvanostatic test, B is from a cell that not had cycled.

cell, but is not sufficiently reliable. Other materials like lithium titanate (LTO) or lithium iron phosphate (LFP) have a more stable potential due to a reversible polarization in a wide current range [31].

#### 4.10.2 The presence of the wire inside the stack

The lithium metal reference is connected outside the cell using a *thick* coated copper wire. The wire it is called *thick* in respect to the other component, in fact electrodes have a thickness less than 50 $\mu\text{m}$  and the separator 20 $\mu\text{m}$ . The wire is 500 $\mu\text{m}$  tick. The introduction of a physical hindrance in a planar system produces damages and distortions in angularity. In figure 4.26A it is shown that where the wire is positioned the active material can be removed or altered. In picture 4.26B, C and D of the same figure, it is shown the effect of the wire on the contact of electrode with separator. In picture B around the wire position the active material of the anode, still wet of electrolyte, have a different color, sign of a different work load. The separator cannot be well stretched and any fold is transferred to the electrode material. For this reason the electrode is not used uniformly and the separator's fold pressed to it, can remove some material.

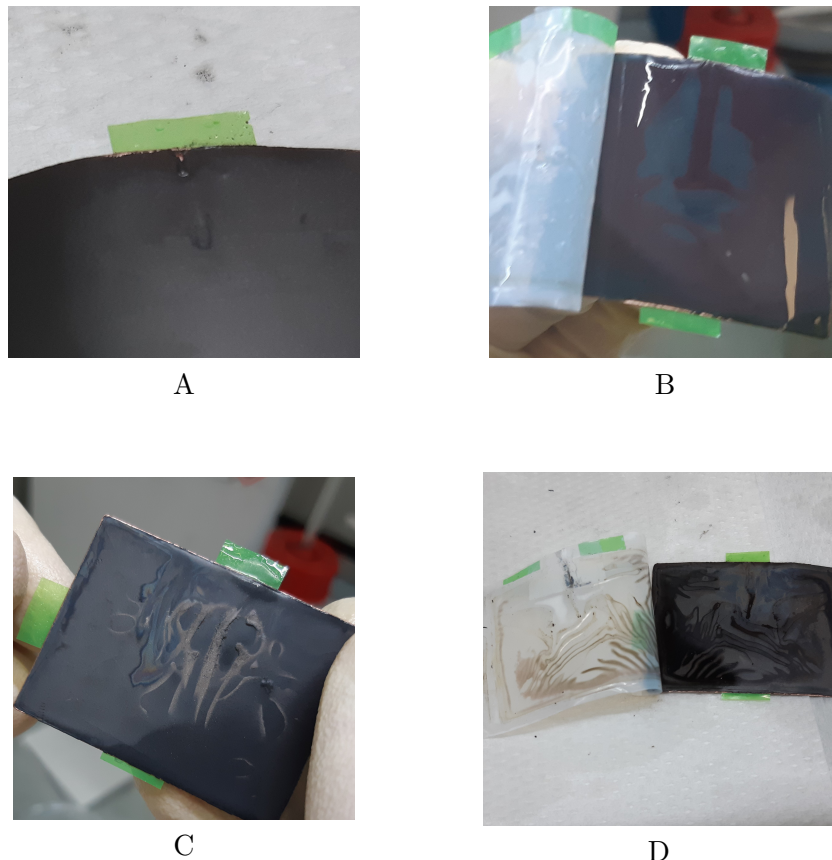


Figure 4.26: Damages inside the cell due to the presence of the wire.

#### 4.10.3 Mechanical issues from anode formulation

As reported in table 3.1, electrodes contain a small percentage of polymeric binder in proportions to what is usually done in laboratory experiments. This produces a lower mechanical resistance and this becomes important for the cell exposed to high pressure. Both in pouch cells under pressure and Swagelok cell types, in the electrolyte was found a considerable quantity of active material dispersed, see figure 4.27. In the galvanostatic test was observed that cell under pressure cannot complete the discharge process because the anode potential increases dramatically (over 3V). Loss of material means that current is distributed to a smaller surface area producing a higher positive overpotential in discharge and the electrodes capacities are no longer balanced. Furthermore anode impedance responses in pouch cells under pressure were found heavily influenced by artifacts (negative loop at low frequency, not reported here).

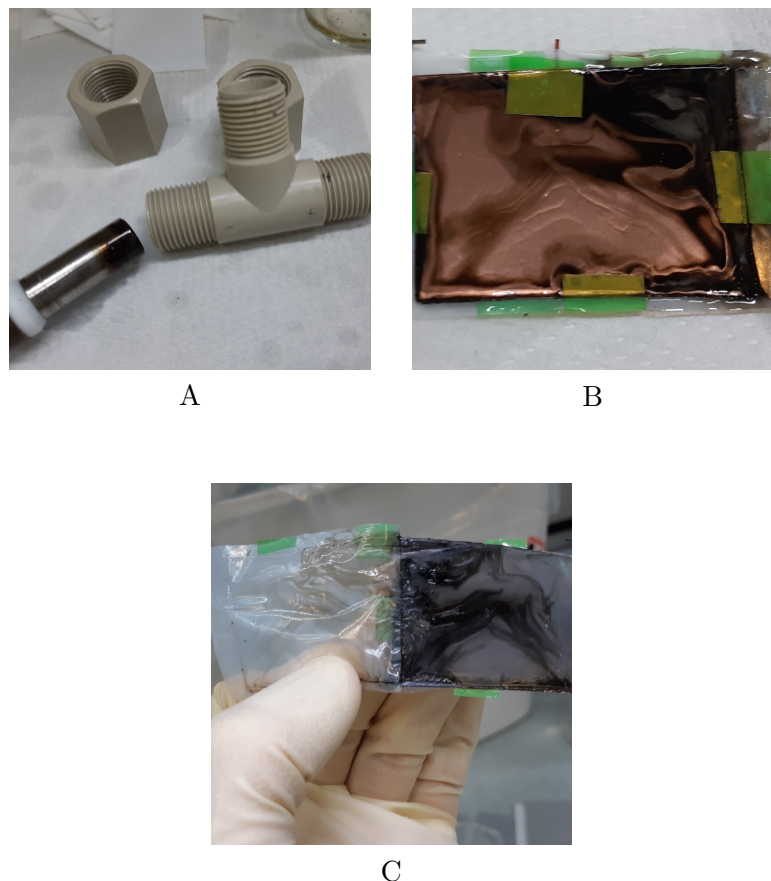


Figure 4.27: Dispersion of the anode material in electrolyte in pouch cells under pressure and Swagelok cell.



## 5 | Conclusions

In this work a complete characterization method is proposed to study battery electrodes in pouch cells. Cell design, experiment set-up with data validation and data elaboration were proposed. The protocol is not yet optimized due to the short time of a thesis project, but all the shortcomings were pointed out and next steps to refine the protocol are easy to define.

With the implementation of the third electrode in a pouch cell, impedance contributes of electrodes were separated and single electrodes behavior can be explored. The goodness of the set-up was ensured with the verification of Kirchhoff's law. With an impedance measure three characteristics resistances can be extracted and they are correlated to ionic conductivity of electrolyte, polarization of current collector/active material interface and charge transfer process. Such phenomena depends on the material, electrode formulation and external conditions (mainly temperature). A robust method to quantify this mechanisms is a powerful tool to study and develop materials.

The main result of the work was the study of temperature dependency of NMC622 cathode impedance with the method illustrated. NMC622 is an important material to understand because it belongs to the upcoming generation 3a of Europe road-map of battery electrodes development. Analyzing the temperature behavior of cathode resistances provides activation energies of mechanisms cited above. Activation energies can be used to compare different systems or to study the microscopic phenomena via theoretical/computational approach. Furthermore Spectroscopy Impedance measurements performed at high temperature give insight of the degradation mechanisms, like dissolution of nickel that is of strong interest at the moment.

The third electrode is also a tool to measure the absolute

potential of electrodes during cell operation. Since no current passes through the reference, but it is only used to probe potential drops, its interface is in electrochemical equilibrium and the potential measurement is unbiased from overpotential contribution. In a standard two-electrodes configuration, the cell is charged and discharge between two fixed voltage value. The full cell voltage is strongly biased by overpotential and is not possible to know if the cell is completely discharged or can be charged more, specially at high C-rate. With the information of single electrode potentials, charge and discharge can be extended without damaging the materials.

A comprehensive method for characterization of electrode in pouch cell format from device realization to data regression, is not present in literature at the moment. The pouch cell is relatively new geometry and it is challenging to build in reproducible way by hand in laboratory. However the pouch cell is a real commercial form factor and so it is easier and more significant to make research in the same geometry.

Next step of this research would be a deep study of the pressure to find the best value to ensure good battery performance and reproducibility. Then a more suited theoretical function has to be developed and the method has to be applied to different materials to address its potentiality.

This characterization approach is applicable for both basic research, industrial R&D and battery state of health diagnosis. Promising results and vast applicability are a drive to pursue this research path with excitement.

# Appendices



# A | MATLAB script for EIS data validation

In this appendix is reported the in-home built script to validate impedance data through regression of a function describing a circuit made of Voigt elements, in MATLAB. The script used to generate initial parameters is at the end of this appendix.

```
%% IMPEDANCE DATA VALIDATION
% Complex non-linear regression of Impedance Spectroscopy data with an
% equivalent circuit built with a finite number of Voigt elements

% Notes: - Overwrite the correct name of the txt file and path
%         - Decimals must be point separated
%         - Data file must not have headers
%         - A file containing starting parameters must be present
%             (use rnd_par_gen.m)
%         - Choose the number of Voigt elements up to 17, in
%             the function definition at the end of the script

clear all
close all

options = optimset('Display','iter','PlotFcns',@optimplotfval);

%% Import data from text file.
% Composition of the data file:
% First column must be frequency in Hz.
% Second column must be real impedance in Ohm.
% Third column must be minus imaginary impedance in Ohm.

path='C:\Data\'; % Path of the data file
fileName='fileName'; % Data filename without extention
Z_d = load([path,fileName,'.txt']);
% Save frequency in a separate vector for later use
omega=Z_d(:,1);
```



```

hold on
plot((omega),res_re,'-k','LineWidth',1.5)
plot((omega),res_im,'—k','LineWidth',1.5)
hold off
set(gca, 'xscale', 'log', 'FontSize',18)
xlabel('omega_(Hz)', 'Interpreter', 'tex', 'FontSize',24)
ylabel('Residuals %', 'FontSize',24)
xlim([omega(length(omega)) omega(1)])
ylim([-1 1])
legend('Real', 'Imaginary')
box on

%% Plotting fitting
figure('Position',[0 0 800 800])
hold on
plot(Z_v(:,2),Z_v(:,3),'k','LineWidth',1.5) % Impedance from model
scatter(Z_d(:,2),Z_d(:,3),'ok') % Impedance from data
hold off
set(gca, 'FontSize',24)
m=Z_d(length(omega),2);
axis equal
xlim([0 ceil(m)])
ylim([0 ceil(m)])
xlabel('Z_{Re}(\Omega)', 'Interpreter', 'tex', 'FontSize',24)
ylabel('Z_{Im}(\Omega)', 'Interpreter', 'tex', 'FontSize',24)
legend('Voigt fit', 'Data', 'FontSize',24)
box on

%% Define the parametric function for general circuit
% with n Voigt elements
function y=fun(omega,par)
v1=par(2)./(1+1i*omega*par(2)*par(3));
v2=par(4)./(1+1i*omega*par(4)*par(5));
v3=par(6)./(1+1i*omega*par(6)*par(7));
v4=par(8)./(1+1i*omega*par(8)*par(9));
v5=par(10)./(1+1i*omega*par(10)*par(11));
v6=par(12)./(1+1i*omega*par(12)*par(13));
v7=par(14)./(1+1i*omega*par(14)*par(15));
v8=par(16)./(1+1i*omega*par(16)*par(17));
v9=par(18)./(1+1i*omega*par(18)*par(19));
v10=par(20)./(1+1i*omega*par(20)*par(21));
v11=par(22)./(1+1i*omega*par(22)*par(23));
v12=par(24)./(1+1i*omega*par(24)*par(25));
v13=par(26)./(1+1i*omega*par(26)*par(27));
v14=par(28)./(1+1i*omega*par(28)*par(29));

```

```
v15=par(30)./(1+1 i*omega*par(30)*par(31));
v16=par(32)./(1+1 i*omega*par(32)*par(33));
v17=par(34)./(1+1 i*omega*par(34)*par(35));

% Modify this with the chosen number of Voigt elements
y=par(1)+v1+v2+v3+v4+v5+v6+v7+v8+v9+v10+v11+v12+v13+v14+v15+v16+v17;

end
```

## Initial parameters generator

```
% Random parameter generator for data validation
% Generate a text file with 36 random number from 0 to 1
```

```
fileName='fileName';
path='C:\Data\';
n=36;
M=rand([n 1]);
dlmwrite([path,fileName,'.txt'],M,'delimiter','\t')
```



## B | MATLAB script for EIS data regression

Below is reported the in-home built MATLAB script for the complex non-linear regression of a theoretical impedance function to experimental data.

```
%% NONLINEAR FITTING OF POURUS ELECTRODES IMPEDANCE
% Ipedance of porus electrodes is fitted using a Complex Non-Linear
% Regression. The theoretical function used is from

clear all
close all
options = optimset('Display','iter','PlotFcns',@optimplotfval);

%% Import data from text file.
% Notes: - Overwrite the correct name of the txt file and path
%         - Decimals must be point separated
%         - Data file must not have headers
%
% Coposition of the data file:
% First coloumn must be frequency in Hz.
% Second coloumn must be real impedance in Ohm.
% Third coloumn must be minus imaginary impedance in Ohm.

path='C:\Data\'; % Path of the data file
fileName='fileName'; % Data filename without extention
Z_d = load([path,fileName,'.txt']);
% Save frequency in a saperate vecotor for later use
omega=Z_d(:,1);

%% Initial estimated parameters
R_HFR = 0.2 ;
R_cont = 4;
Q_cont = 1e-3;
```

```

a_cont = 0.85;
R_pore = 6 ;
R_el = 1e-8;
R_CT = 4 ;
Q_CT = 1e-3;
a_CT = 0.85;
W = 1.24e-02 ;

 $\% \text{ Vector containing estimated parameters}$ 
 $\% \text{ Use previous defined parameters:}$ 
par0 = [R_HFR;...
R_cont;...
Q_cont;...
a_cont;...
R_pore;...
R_el;...
R_CT;...
Q_CT;...
a_CT;...
W];

 $\% \text{ Import parameters from a file:}$ 
 $\% \text{ par0} = \text{load}([\text{'par\_min}\backslash\text{fit\_par\_}' , \text{fileName} , \text{'.txt'}]);$ 

 $\% \text{ Upper and lower bounds of parameters}$ 
UB = [ -inf ,...
-inf ,...
-inf ,...
1 ,...  $\% a\_cont$ 
-inf ,...
-inf ,...
-inf ,...
-inf , ...
1 ,...  $\% a\_CT$ 
-inf ];
LB = [ 0 ,...
0 ,...
0 ,...
0.5 ,...  $\% a\_cont$ 
0 , ...
0 ,...
0 ,...
0 ,...
0 ,...
0.5 ,...  $\% a\_CT$ 
0 ];

```

```

%% Minimization of sum of the squares
% Sum of squares with a modulus weighting
sum_of_sqr= @(omega,par) ...
    sum( ((real(fun(omega,par))-Z_d(:,2)).^2 ... % Real
        +(-imag(fun(omega,par))-Z_d(:,3)).^2) ... % Imaginary
        ./((Z_d(:,2).^2+Z_d(:,3).^2)) ... % Weighting factor
    );
    
% Minimization function
[par_min, chisq] = fminsearchbnd(@(par) ...
    sum_of_sqr(omega,par),par0,LB,UB,options);

% Normalize chi^2 on number of data point minus the number
% of free parameters
chisq=chisq/(length(omega)-10);

% Save minimum parameters in a txt file
dlmwrite([path,fileName,'.txt'],par_min,'delimiter','\t');

% Calculate theoretical function with minimized parameters
Z_t(:,1)=omega;
F=fun(omega,par_min);
Z_t(:,2)=real(F);
Z_t(:,3)=-imag(F);

%% Compute and plot fitting error residue
% Residues of real part
res_re=100.*((Z_d(:,2)-Z_t(:,2))./Z_d(:,2));
% Residues of imaginary part
res_im=100.*((Z_d(:,3)-Z_t(:,3))./Z_d(:,3));
figure('Position',[0 0 1500 400])
hold on
plot((omega),res_re,'-','Color',[0 0.4470 0.7410],'LineWidth',1.5)
plot((omega),res_im,'-','Color',[0.4660 0.6740 0.1880],'LineWidth',1.5)
hold off
set(gca,'xscale','log','FontSize',18)
xlabel('\omega_(Hz)', 'Interpreter','tex','FontSize',24)
ylabel('Residuals %', 'FontSize',24)
xlim([omega(length(omega)) omega(1)])
ylim([-1 1])
legend('Real','Imaginary')
box on

%% Plotting fit with data

```

```

figure('Position',[0 0 800 800])
hold on
plot(Z_t(:,2),Z_t(:,3),'k','LineWidth',1.5) % Impedance from model
scatter(Z_d(:,2),Z_d(:,3),'o') % Impedance from data
hold off
set(gca, 'FontSize',24)
m=Z_d(length(omega),2);
axis equal
xlim([0 ceil(m)])
ylim([0 ceil(m)])
xlabel('Z_{Re}(\Omega)', 'Interpreter','tex', 'FontSize',24)
ylabel(' - Z_{Im}(\Omega)', 'Interpreter','tex', 'FontSize',24)
legend('Fit','Data','FontSize',24)
box on

%% Print in command line minimum parameters
fprintf([ 'Minimized_parameters:\n' ...
'R_HFR=%2e Ohm\n' ...
'R_cont=%2e Ohm\n' ...
'Q_cont=%2e F*s\n' ...
'a_cont=%2e\n' ...
'R_pore=%2e Ohm\n' ...
'R_el=%2e Ohm\n' ...
'R_CT=%2e Ohm\n' ...
'Q_CT=%2e F*s\n' ...
'a_CT=%2e\n' ...
'W=%2e Ohm*s^{(-1/2)}\n' ...
'Chi^2=%f\n' ],...
par_min(1), par_min(2), par_min(3), par_min(4), par_min(5), par_min(6),...
par_min(7), par_min(8), par_min(9), par_min(10), chisq)

%% Function for the regression
function y = fun(omega,par)
RHFR = par(1); % High frequency intercept
Rcont = par(2);
Qcont = par(3);
acont = par(4);
Rpore = par(5);
Rel = par(6); % Electric resistance of metal collector
Rct = par(7);
Qct = par(8);
act = par(9);
W = par(10);

ni = sqrt((Rct*Qct*(1i*omega).^act +1)*(Rpore+Rel)/Rct);

```

```
p = Rpore/(Rpore+Rel);  
s = 1-p;  
Z_str = sqrt(Rct*(Rpore+Rel)./(Rct*Qct*(1i*omega).^act +1)); % Z*  
Zpore = s*p*(Rpore+Rel) + ...  
Z_str.*(1+2*p*s.*sqrt(1-(tanh(ni)).^2)-1)./(tanh(ni));  
Zcon = Rcont*(Rcont*Qcont*(1i*omega).^acont + 1).^ -1;  
Zw = W./sqrt(omega)-1i.* (W./sqrt(omega));  
y = RHFR + Zpore + Zcon + Zw ; % Z_tot  
  
end
```



# C | Results of complex non-linear regressions

In this appendix are reported the results for the regression of cathode impedance for Pouch 3 cell, performed at different temperatures.

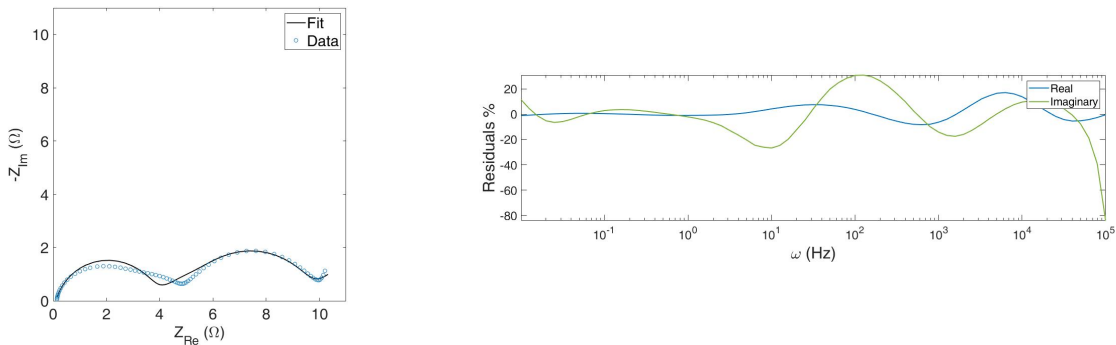


Figure C.1: Cathode impedance, performed at 30°C under 2.7kPa.

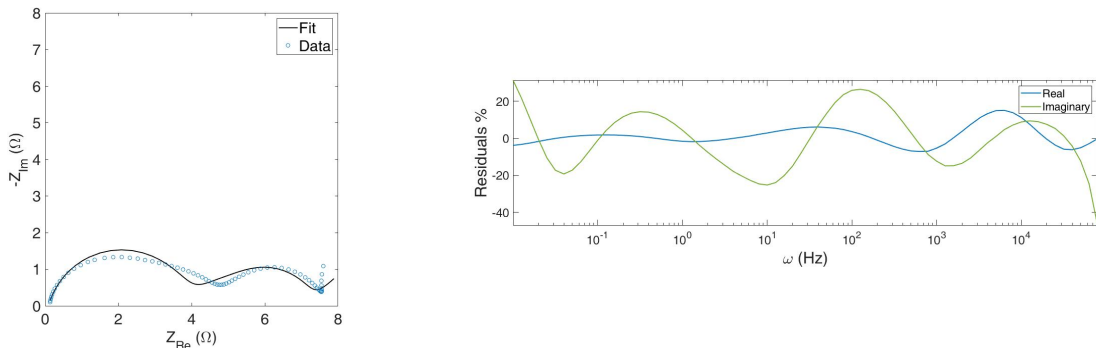


Figure C.2: Cathode impedance, performed at 40°C under 2.7kPa.

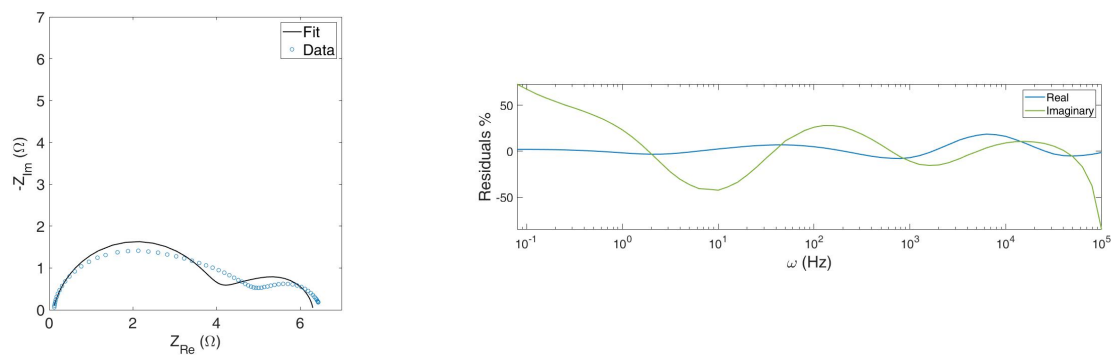


Figure C.3: Cathode impedance, performed at 50°C under 2.7kPa.

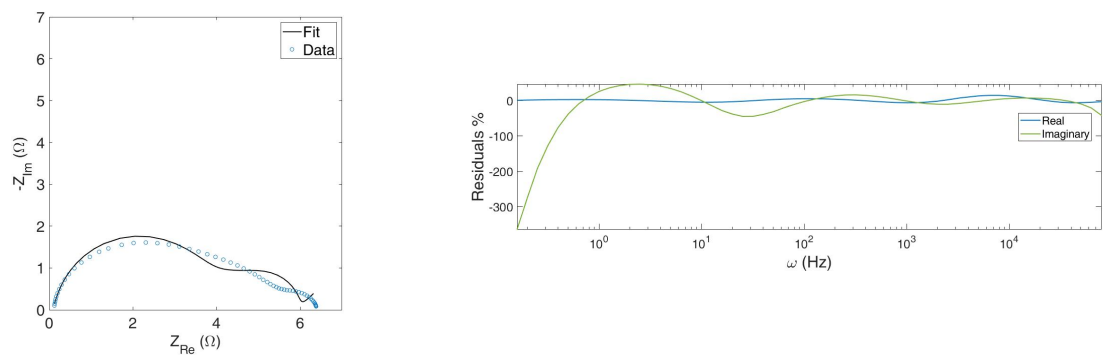


Figure C.4: Cathode impedance, performed at 60°C under 2.7kPa.

## References

- [1] Martin Winter and Ralph J Brodd. *What are batteries, fuel cells, and supercapacitors?* 2004.
- [2] Susumu Yoda and Kaoru Ishihara. “The advent of battery-based societies and the global environment in the 21st century”. In: *Journal of Power Sources* 81 (1999), pp. 162–169.
- [3] Gianfranco Pistoia. *Batteries for portable devices*. Elsevier, 2005.
- [4] David C Bock et al. “Batteries used to power implantable biomedical devices”. In: *Electrochimica acta* 84 (2012), pp. 155–164.
- [5] I Tsiropoulos, D Tarvydas, and N Lebedeva. “Li-ion Batteries for Mobility and Stationary Storage Applications Scenarios for Costs and Market Growth”. In: *Publications Office of the European Union: Luxembourg* (2018).
- [6] Marc Steen et al. “EU competitiveness in advanced Li-ion batteries for E-mobility and stationary storage applications—opportunities and actions”. In: *JRC Science for Policy Report* (<https://goo.gl/BPyJbt>) (2017).
- [7] European Commission. “A clean planet for all. A European strategic long-term vision for a prosperous, modern, competitive and climate neutral economy”. In: *COM (2018) 773 final* (2018).
- [8] Nationale Plattform Elektromobilität. “Roadmap integrierte Zell-und Batterieproduktion Deutschland”. In: Herausgeber: Gemeinsame Geschäftsstelle Elektromobilität der Bundesregierung (GGEMO). Berlin: GGEMO (2016).
- [9] Matthew Li et al. “30 years of lithium-ion batteries”. In: *Advanced Materials* 30.33 (2018), p. 1800561.
- [10] Colin Vincent and Bruno Scrosati. *Modern batteries*. Elsevier, 1997.
- [11] John O’M Bockris, Amulya KN Reddy, and Maria Gamboa-Aldeco. *Modern Electrochemistry: Fundamentals of Electrodics. V. 2a*. Plenum Press, 1998.
- [12] Xiangkun Wu et al. “Safety Issues in Lithium Ion Batteries: Materials and Cell Design”. In: *Frontiers in Energy Research* 7 (July 2019). DOI: [10.3389/fenrg.2019.00065](https://doi.org/10.3389/fenrg.2019.00065).
- [13] Scott Lemon and Allan Miller. “Electric Vehicles in New Zealand: Technologically Challenged?” In: June 2013.
- [14] Yemeserach Mekonnen, Aditya Sundararajan, and Arif Sarwat. “A review of cathode and anode materials for lithium-ion batteries”. In: Mar. 2016, pp. 1–6. DOI: [10.1109/SECON.2016.7506639](https://doi.org/10.1109/SECON.2016.7506639).
- [15] Tsutomu Ohzuku and Yoshinari Makimura. “Layered lithium insertion material of LiCo<sub>1/3</sub>Ni<sub>1/3</sub>Mn<sub>1/3</sub>O<sub>2</sub> for lithium-ion batteries”. In: *Chemistry Letters* 30.7 (2001), pp. 642–643.
- [16] Zhonghua Lu, DD MacNeil, and JR Dahn. “Layered cathode materials Li [Ni<sub>x</sub>Li<sub>(1/3-x/3)</sub>Mn<sub>(2/3-x/3)</sub>]O<sub>2</sub> for lithium-ion batteries”. In: *Electrochemical and Solid-State Letters* 4.11 (2001), A191–A194.
- [17] Roland Jung et al. “Oxygen Release and Its Effect on the Cycling Stability of LiNi<sub>x</sub>Mn<sub>y</sub>Co<sub>z</sub>O<sub>2</sub> (NMC) Cathode Materials for Li-Ion Batteries”. In: *Journal of The Electrochemical Society* 164 (Jan. 2017), A1361–A1377. DOI: [10.1149/2.0021707jes](https://doi.org/10.1149/2.0021707jes).
- [18] Jiangfeng Qian et al. “High rate and stable cycling of lithium metal anode”. In: *Nature communications* 6.1 (2015), pp. 1–9.
- [19] Chu Liang et al. “Lithium alloys and metal oxides as high-capacity anode materials for lithium-ion batteries”. In: *Journal of alloys and compounds* 575 (2013), pp. 246–256.

- [20] Sheng Shui Zhang. “A review on the separators of liquid electrolyte Li-ion batteries”. In: *Journal of power sources* 164.1 (2007), pp. 351–364.
- [21] Ganesh Venugopal et al. “Characterization of microporous separators for lithium-ion batteries”. In: *Journal of power sources* 77.1 (1999), pp. 34–41.
- [22] Pallavi Verma, Pascal Maire, and Petr Novák. “A review of the features and analyses of the solid electrolyte interphase in Li-ion batteries”. In: *Electrochimica Acta* 55.22 (2010), pp. 6332–6341.
- [23] L El Ouatani et al. “The effect of vinylene carbonate additive on surface film formation on both electrodes in Li-ion batteries”. In: *Journal of The Electrochemical Society* 156.2 (2009), A103–A113.
- [24] Arianna Moretti et al. “A Comparison of Formation Methods for Graphite//LiFePO<sub>4</sub> Cells”. In: *Batteries & Supercaps* 2.3 (2019), pp. 240–247.
- [25] URL: <https://el-cell.com/>.
- [26] Andrzej Lasia. “Electrochemical impedance spectroscopy and its applications”. In: *Modern aspects of electrochemistry*. Springer, 2002, pp. 143–248.
- [27] Francisco Sepúlveda, José Hernández, and Andrés Manríquez. “Construction of a Potentiostat to Perform Electrochemical Impedance Spectroscopy (EIS) Tests”. In: *Modern Instrumentation* 6.2 (2017), pp. 15–27.
- [28] J Ross Macdonald and E Barsoukov. “Impedance spectroscopy: theory, experiment, and applications”. In: *History* 1.8 (2005), pp. 1–13.
- [29] Andre Leonide, Yannick Apel, and Ellen Ivers-Tiffée. “SOFC modeling and parameter identification by means of impedance spectroscopy”. In: *ECS Transactions* 19.20 (2009), p. 81.
- [30] Dino Klotz. *Characterization and modeling of electrochemical energy conversion systems by impedance techniques*. KIT Scientific Publishing, 2014.
- [31] Rinaldo Raccichini, Marco Amores, and Gareth Hinds. “Critical Review of the Use of Reference Electrodes in Li-Ion Batteries: A Diagnostic Perspective”. In: *Batteries* 5.1 (2019), p. 12.
- [32] Brian Burrows and Raymond Jasinski. “The Li/Li<sup>+</sup> reference electrode in propylene carbonate”. In: *J. electrochem. Soc* 115.4 (1968), pp. 365–367.
- [33] Abdilbari Shifa Mussa et al. “Effects of external pressure on the performance and ageing of single-layer lithium-ion pouch cells”. In: *Journal of Power Sources* 385 (2018), pp. 18–26.
- [34] Da-Wei Wang et al. “3D aperiodic hierarchical porous graphitic carbon material for high-rate electrochemical capacitive energy storage”. In: *Angewandte Chemie International Edition* 47.2 (2008), pp. 373–376.
- [35] Johannes Landesfeind, Daniel Pritzl, and Hubert A Gasteiger. “An analysis protocol for three-electrode li-ion battery impedance spectra: Part i. analysis of a high-voltage positive electrode”. In: *Journal of The Electrochemical Society* 164.7 (2017), A1773–A1783.
- [36] Frederik Michel Dekking et al. *A Modern Introduction to Probability and Statistics: Understanding why and how*. Springer Science & Business Media, 2005.
- [37] URL: <https://it.mathworks.com/matlabcentral/fileexchange/17804-fminsearchbnd-new>.
- [38] Mark E Orazem and Bernard Tribollet. *Electrochemical impedance spectroscopy*. John Wiley & Sons, 2017.
- [39] John S Toll. “Causality and the dispersion relation: logical foundations”. In: *Physical review* 104.6 (1956), p. 1760.

- [40] Jan Philipp Schmidt et al. “Studies on LiFePO<sub>4</sub> as cathode material using impedance spectroscopy”. In: *Journal of Power Sources* 196.12 (2011), pp. 5342–5348.
- [41] Peter G Bruce and MY Saidi. “A two-step model of intercalation”. In: *Solid State Ionics* 51.3-4 (1992), pp. 187–190.
- [42] Matthieu Dubarry, Cyril Truchot, and Bor Yann Liaw. “Synthesize battery degradation modes via a diagnostic and prognostic model”. In: *Journal of power sources* 219 (2012), pp. 204–216.
- [43] Christopher J Seeton. “Viscosity–temperature correlation for liquids”. In: *Tribology letters* 22.1 (2006), pp. 67–78.
- [44] John O’M. Bockris and Amulya KN Reddy. *Modern Electrochemistry, Volume 1: Ionics (Second Edition)*. 2002.
- [45] A Chagnes et al. “Ion transport theory of nonaqueous electrolytes. LiClO<sub>4</sub> in  $\gamma$ -butyrolactone: the quasi lattice approach”. In: *Electrochimica acta* 46.12 (2001), pp. 1783–1791.
- [46] AS Keefe et al. “Temperature Dependent EIS Studies Separating Charge Transfer Impedance from Contact Impedance in Lithium-Ion Symmetric Cells”. In: *Journal of The Electrochemical Society* 166.14 (2019), A3272.
- [47] Lihua Jiang, Qingsong Wang, and Jinhua Sun. “Electrochemical performance and thermal stability analysis of LiN<sub>x</sub>C<sub>y</sub>Mn<sub>z</sub>O<sub>2</sub> cathode based on a composite safety electrolyte”. In: *Journal of hazardous materials* 351 (2018), pp. 260–269.